Influence of sedimentation and detrital clay grain coats on chloritized sandstone reservoir qualities: Insights from comparisons between ancient tidal heterolithic sandstones and a modern estuarine system

Maxime Virolle, Benjamin Brigaud, Sylvain Luby, Éric Portier, Hugues Féniès, Raphaël Bourillot, Patricia Patrier, Daniel Beaufort

Influence of sedimentation and detrital clay grain coats on chloritized sandstone reservoir qualities: Insights from comparisons between ancient tidal heterolithic sandstones and a modern estuarine system

Maxime Virolle[1], Benjamin Brigaud[1], Sylvain Luby[1], Eric Portier[2], Hugues Fenies[3], Raphaël Bourillot[3], Patricia Patrier[4], Daniel Beaufort[4]

[1]GEOPS, Univ. Paris-Sud, CNRS, Université Paris-Saclay, 91405 Orsay, France

[2]Neptune Energy, 9-11 Allée de l'Arche, 92400 Courbevoie, France

[3]Géoressources et Environnement, ENSEGID, Bordeaux INP, Université Bordeaux Montaigne, Pessac 33607, France

[4]IC2MP, CNRS, UMR 7285, TSA 51106, Université de Poitiers, 86073 Poitiers, France

Corresponding author: maxime.virolle@u-psud.fr, GEOPS, Univ. Paris-Sud, CNRS, Université Paris-Saclay, 91405 Orsay, France

Abstract

Authigenic clay coatings (mostly Fe-rich chlorite coatings) affect sandstone reservoir qualities by inhibiting quartz overgrowth during burial diagenesis. It is still unclear what initial mineralogical assemblages and initial sedimentation conditions produce chloritized sandstone reservoirs. To address this question, sedimentological, petrographical and mineralogical analyses were carried out for both a deeply buried Permian estuarine

sandstone reservoir (Australia) and the Gironde estuary (France). Comparisons reveal similar sedimentary facies and vertical facies associations, indicative of tidal sand bars deposited in a mud-rich estuary. The two sedimentary systems display clay layers several metres thick corresponding to fluid mud deposits at the bottom of the estuary channel. Detrital clay grain coats composed of illite, smectite, kaolinite and chlorite are observed in the modern Gironde tidal bars while Fe-rich chlorite coatings are observed in the Permian deposits. Transformations of detrital clays into other clay minerals (such as berthierine) during eogenesis can initiate well-crystallized Fe-rich chlorite formation during burial diagenesis. The release of iron within water formations during eogenesis could enhance the subsequent precipitation of berthierine, which may be the precursor to Fe-rich chlorite. Our results also indicate that facies from the middle to the upper sand bar at the top of the transgressive cycle were probably uncemented during burial. This is partly due to the initial clay fraction content of 15–20%, part of which forms detrital clay grain coats. Detrital minerals and detrital clay grain coats observed in the Gironde estuary could be the prerequisite initial conditions for generating Fe-rich chloritization in estuarine sandstones during burial. The use of an analogous data set appears to be fundamental in building a predictive capability for clay coat-derived, high reservoir quality in deeply buried sandstones.

Keywords: Detrital clay, Chloritization, Reservoirs, Estuarine sandstones

1. Introduction

Factors controlling reservoir quality and heterogeneity – porosity (phi) and permeability (k) – are prerequisites for improving modelling and for forecasting geothermal potential and oil or gas reserves. Quartz cementation is one of the main processes degrading reservoir quality in clastic rocks (Bjorlykke and Egeberg, 1993; Worden and Morad, 2000). However, authigenic

clay coatings, mainly chlorite, may limit quartz overgrowth diagenesis and thereby maintain reservoir quality during burial (Heald and Larese, 1974; Pittman et al., 1992; Ehrenberg, 1993; Aase et al., 1996; Bloch et al., 2002). Both the proportion of the quartz grain surface covered by clay minerals (i.e. clay-coat coverage) and the coating mineralogy are crucial for the preservation of porosity (Billault et al., 2003; Lander et al., 2008, Griffiths, 2018). With extensive coat coverage by chlorites, less quartz cement nucleates (Heald and Larese, 1974; Walderhaug, 1996). Clay coatings may have developed in a wide variety of depositional environments (Worden and Morad, 2003; Dowey et al., 2012, Wooldridge et al., 2017a, 2018, Griffiths et al., 2018). Shallow-marine water depositional environments, such as estuarine environments, form numerous heterolithic sandstone reservoirs (Wood, 2004; Martinius et al., 2005; Musial et al., 2012; Massart, 2014). The reservoir quality of these estuarine reservoirs is partly controlled by grain coating development during diagenesis (Worden and Morad, 2003; Morad et al., 2010; Dowey et al., 2012; Saïag et al., 2016). Well-crystalized chlorite or illite coatings can originate either from direct precipitation from aqueous solutions (neoformation) without clay material precursors (Haile et al., 2015; Mamadou et al., 2016), or from thermally driven transformations of precursors (Aagaard et al., 2000). Well-crystalized clay coatings begin to develop during low-temperature diagenesis (30–70 °C) from the transformation of clay precursors such as berthierine or odinite for chlorite coatings (Wilson and Pittman, 1977; Hillier, 1994; Aagard et al., 2000; Worden and Morad, 2003; Morad et al., 2010; Beaufort et al., 2015). This transformation might be enhanced by feldspar dissolution and the availability of iron in the sedimentary system (Morad et al., 2010; Khalifa and Morad, 2012; Haile et al., 2015; Daneshvar and Worden, 2018).

In the initial depositional environment, clays may be incorporated within the sediments

during or shortly after deposition (Griffiths et al., 2018, Virolle et al., 2019). Detrital clay minerals can form coats around grains (Wooldridge et al., 2018, Griffiths et al., 2018; Virolle et al., 2019). They may thus contribute to forming the precursors required for the chloritization process during burial diagenesis (Gould et al., 2010; Dowey et al., 2017). In the estuarine Permian Cape Hay Formation, densely packed clay mineral aggregates are observed beneath or close to the well-crystallized coating with more euhedral and more widely spaced chlorite crystals (Saïag et al., 2016). Those aggregates might be the relic of clay precursors, suggesting chlorite coating nucleation in clastic sand during burial (Gould et al., 2010; Saïag et al., 2016). Various processes have been described to explain the incorporation of clays within sand grains during or just after deposition. For example, through sediment mixing during bioturbation, mechanical infiltration of muddy waters, tidal pumping in coastal environments, or even through interactions with exopolymeric substances produced by diatoms acting as glue (Herringshaw and McIlroy, 2013; Pittman et al., 1992; Walker, 1976; Walker et al., 1978; Worden and Morad, 2003; Wooldridge et al., 2017a, 2017b). Such detrital coats have been described in the modern Gironde and Ravenglass estuaries in sand bar sequences or on sand flats (Dowey et al., 2017; Woolridge et al., 2017a, 2018; Griffiths et al., 2018, 2019; Virolle et al. 2019). Uncertainties exist as to the influence of sedimentation on chloritized sandstone reservoir qualities. Besides, it remains unclear how to associate the occurrence and proportion of coats with a specific sedimentary facies type such as intertidal, supratidal, lower or upper sand bars, proximal or distal bay-head deltas (Wooldridge et al., 2017a; Griffiths et al., 2018 Virolle et al., 2019). A recent study of a modern analogue in the United Kingdom (Ravenglass) shows that chlorite-enriched tidal bars and dunes of an inner estuary might experience a low cementation rate during burial with their well-developed detrital clay coats (Griffiths et al., 2019). Another

uncertainty arises over coat development in coastal environments within the stratigraphic cycle. Linking tidal facies types with the presence of clay in optimum proportions within sequence stratigraphy is fundamental to improving the prediction of clay coating and reservoir location in coastal sandstones.

This study proposes to compare a Permian estuary, and more specifically the Cape Hay Formation (Australia) buried at great depth (3600 m), with the Gironde estuary (South-West France) as a modern analogue to link sedimentary facies with clay coats and reservoir quality. The ultimate aim is to identify and precisely locate the tidal sedimentary facies in an estuarine environment and/or in sequence stratigraphy that may have the best reservoir qualities. This prediction must integrate the presence of clays as coats and clay heterogeneities in sand estuarine facies.

The Upper Cape Hay Formation (Petrel sub-basin, part of the Bonaparte Basin in Australia) is revisited to detail very precisely the sedimentary facies and the occurrence of coating. This sedimentary formation was deposited during the Permian and during a third-order transgressive period within a tide-dominated environment with tidal sand bar deposits (Kloss et al., 2004; Saïag et al., 2016). The link between the preservation of high porosity and permeability values observed in this geological formation and the development of clay coatings (mostly Fe-rich chlorite) during early diagenesis has been clearly demonstrated by Saiag et al. (2016) because coatings prevent quartz overgrowth during burial.

The Gironde estuary is a mud-rich macrotidal estuary (Sottolichio et al., 2011; Jalon-Rojas et al., 2016). Tidal bars forming the bay-head delta observed within the Gironde estuary are large, elongate and asymmetrical (Féniès and Tastet, 1998; Virolle et al., 2019). They may be several kilometres wide, tens of kilometres long and tens of metres high (25 to 50 m; Dalrymple and Rhodes, 1995; Berne et al., 1998; Féniès and Tastet, 1998; Dyer and Huntley,

1999; Reynaud et al., 1999; Wood, 2003; Dalrymple and Choi, 2007; Leuven et al., 2016; Aschoff et al., 2018). Two tidal bars have been studied in detail, the Plassac and the Richard tidal bars located in the inner and outer estuary funnel respectively. The comparison is based on the study of six cores from the Gironde estuary tidal bars (for a total of 31 m) and detailed descriptions of cores (28 m) from one well in a set of six wells from the Permian Upper Cape Hay Formation (P.U.C.H.F.) within the Petrel sub-basin. The analogy will provide a better understanding of the distribution and prediction of well-preserved porosity and permeability layers within deeply buried sandstone reservoirs.

2. Geological settings

2.1 Petrel sub-basin

The Petrel gas field is located offshore (95 m below sea level), 260 km west-southwest of Darwin city in northern Australia, on the border between Western Australia and the Northern Territory (Fig. 1A; Earl, 2004). It is located in the Joseph Bonaparte Basin, in the centre of the Petrel sub-basin (Earl, 2004; Zhixin et al., 2012; Seebeck et al., 2015). The Bonaparte Basin covers an area of 270,000 km² and forms a province of the hydrocarbon-rich north-western Australian shelf. The inferred resources are: 938 million barrels of oil, 1901 million barrels of condensate and 975 trillion cubic metres of natural gas (Zhixin et al., 2012).

Most of the hydrocarbon reservoirs of the Petrel sub-basin are in the Permian formations. Lithostratigraphically, they are composed of the Treachery Shale, Keyling Formation, Fossil Head Formation, and the Hyland Bay subgroup (Fig. 1B; Bhatia et al., 1984). The Hyland Bay subgroup consists of five geological formations (Gorter, 1998): Pearce, Cape Hay, Dombey,

Tern and Penguin (Fig. 1B). The Petrel gas field reservoir is located in the Upper Cape Hay Formation (Fig. 1B). This formation is a succession of shallow-marine, coastal to fluvial environments within a second-order regression-transgression cycle (Saiag et al., 2016). The source rocks are continental in nature and were also deposited during the Permian (Pearce Formation, Keyling Formation). The Petrel gas field is an extended anticline (30 km by 15 km) oriented NW–SE, and 60 m thick. A total of seven boreholes were drilled including 275 m of cores in the Cape Hay Formation (Kloss, 2004; Saïag et al., 2016).

The sandstones studied belong to the upper part of the Cape Hay Formation composed of deeply buried tidal deposits (>3500 m; pressures of 350 bars and temperatures of 130 °C). They exhibit wide ranges of porosity (2–26%) and permeability (0.001–2500 mD) (Bhatia et al., 1984; Kloss et al., 2004; Saïag et al., 2016). Saiag et al. (2016) have demonstrated that the preservation of high porosity and permeability values are linked to clay coatings (mostly Fe-rich chlorite). The depositional environment of the Upper Cape Hay Formation, the gas reservoir target, is described as a tide-dominated estuary with tidal sand bar deposits (Fig. 1C; Kloss et al., 2004; Saïag et al., 2016).

2.2 The Gironde estuary

The Gironde estuary in south-west France is one of the largest estuaries in Europe (Fig. 2A; Dalrymple and Rhodes, 1995). The estuary funnel is 75 km long and covers an area of 630 km^2 (Fig. 2A). The estuarine tidal channels (Dordogne and Garonne channels) extend over 85 km inland from the estuary funnel (Fig. 2A). The estuary is divided into three main sections differentiated by their morphological and hydrodynamic characteristics (Fig. 2A; Allen, 1973; Allen, 1991).

(1) The estuarine channels are composed by the Garonne and Dordogne. The Garonne estuary channel extends inland from the estuary funnel as far as the upstream tidal limit near La Réole some 160 km from the estuary mouth (Fig. 2A). Estuarine heterolithic point bars can be observed along a large part of these channels.

(2) The landward part of the Gironde inner estuary funnel is occupied by the bay-head delta (Allen, 1991; Féniès and Tastet, 1998), composed of several tidal bars including the Plassac tidal bar (Fig. 2A-B). The estuary funnel is mainly composed of tidal bars and estuarine mud (Fig. 2A).

(3) The Gironde outer estuary funnel consists of a tidal inlet channel and a muddy central basin located further inland (Fig. 2A). The Richard tidal bar is located in this area (Fig. 2A and C).

The Gironde is a mud-rich macrotidal estuary with a well-developed Turbidity Maximum Zone (TMZ) that corresponds to highly turbid waters (Allen and Castaing, 1973; Doxaran et al., 2009; Sottolichio et al., 2011). It is a zone with a high concentration of suspended matter, extending 70 to 80 km along the estuary. Its concentration fluctuates from 1 to 10 g.l at the water surface to hundreds of g.l on the estuary bottom (Allen and Castaing, 1973; Allen et al., 1977). The formation of the TMZ results from two mechanisms: density-driven circulation (saline and fresh water) and the hypersynchronous nature of the estuary (Allen, 1991). Both mechanisms contribute to the trapping of fine particles and to the formation of the TMZ. The TMZ position shifts in the estuary due to the seasonal cycle of fluvial discharge (Doxaran et al., 2009). Clay minerals in the suspended matter are, on average, composed of illite (49%), smectite (22%), kaolinite (14%) and chlorite (15%) (Jouanneau and Latouche, 1981).

3. Material and Methods

3.1 Facies descriptions

Facies descriptions for the P.U.C.H.F. were made on high-resolution pictures provided by Neptune Energy. The study focused on the detailed description of the Petrel E well for which 28 m of cores have been described. Descriptions were made at one-tenth scale. For the Gironde estuary tidal bars, facies were described on the same scale on cores extracted from the Plassac and the Richard tidal bars (Fig. 2B-C). Cores were extracted from an east–west transect, perpendicular to the long axis of the tidal bars (Fig. 2B-C). On the Plassac tidal bar (45°06'24.49''N 0°39'37.87''W) three cores (PLA-2015-E, PLA-2015W and PLA-2015C for East, West and Centre) were extracted at about 150 m intervals (Fig. 2B). Core lengths vary from 4.44 m to 6.70 m for a total length of about 16 m. The three cores (Ri-2016-E, Ri-2016-W and Ri-2016-C) of the Richard tidal bar were extracted along a 90 m long transect, with depths ranging from 4.60 m to 6.50 m and for a total length about 15 m (Fig. 2C).

3.2 Petrographic descriptions

A total of 38 plugs from the P.U.C.H.F. (27 were used for petrographic analyses and 33 for mineralogical analyses), and 85 plugs (diameter: 4 cm) from the Gironde estuary (53 from the Plassac tidal bar and 32 from the Richard tidal bar) were analysed. The sampling in the Gironde estuary was carried out while the sediments were still wet and cohesive so as to preserve sedimentary structures. The plugs from the Gironde were dried in a heat chamber at 40 °C for 24 hours and then indurated with blue epoxy resin under a low vacuum to preserve the sedimentary structures and rock fabric. Standard polished thin sections (30 μm thick) were then made from the indurated plugs.

Thin sections of resin-impregnated samples were observed under a Nikon Eclipse Ci-POL (Nikon, Tokyo, Japan) and a Leica DM 750P (Leica Microsystems, Wetzlar, Germany)

polarizing microscope to characterize the microfacies. In each thin section, the relative surface area (%) of the pores (macroporosity) and the sediment components were quantified using random grid point counting with JmicroVision Image analysis software (Roduit, 2007). A minimum of 300 counts were performed on 20 different images (2.5 mm x 2.5 mm) in each thin-section. Several categories were distinguished based on whether the study involved the modern environment or the deeply buried sandstone reservoir: detrital clay grain coats, quartz (coated and non-coated), feldspars (coated and non-coated), lithics (coated and non-coated), clay matrix, biotite, muscovite, bioclasts, pyrite, quartz overgrowth, macroporosity (primary and secondary porosity), pore filling, clay cement and carbonated cement.

In the Gironde estuary samples, grain coat coverage was quantified by determining the proportion of the outer perimeter of the grains that was coated relative to the total surface area (coated and non-coated). The coated grains category was divided into four sub-categories depending on the grain coat coverage of the grain surface: (i) 1 to 5%; (ii) 5 to 15%; (iii) 15 to 30%; and (iv) more than 30%.

In the P.U.C.H.F., coat coverage was analysed by considering surfaces where quartz overgrowths could nucleate and surfaces with coatings. Surfaces were excluded if they were in contact with neighbouring grains, the detrital matrix, or pore-filling cement formed before quartz cementation.

Scanning electron microscopy (SEM) was performed on thin sections and on individual sand grains mounted on 1 cm diameter stubs. Samples were gold and palladium coated. Observations and pictures were made in backscattered electron mode (BSE) with a Phenom X Pro SEM (Phenom-World B.V., Eindhoven, The Netherlands), at 10 keV in imaging conditions and 15 keV for elementary analyses.

Grain size measurements were performed using a Mastersizer 2000 laser granulometer (Malvern, Worcestershire, UK) for the Gironde estuary samples, and using J-Microvision (100 measurements per thin section in point counting) for the P.U.C.H.F. samples. Mean grain size was calculated using Folk's (1980) equation:

Mz =(ø16 + ø50 + ø84)/3, where ø16, ø50 and ø84 correspond to particle diameter (mm) in ø units (ø = -log2) at 16, 50 and 84% of the grain size distribution.

Sorting was calculated using standard deviation øi defined by Folk and Ward (1957):

øi=(ø84 − ø16)/4+(ø95 − ø5)/6.6, where ø5, ø 16, ø84 and ø95 correspond to particle diameter (mm) in ø units (ø = -log2) at 16, 50 and 84% of the grain size distribution. Mud was used to characterize the grain-size fraction less than 63 (µm), i.e. silts plus clays.

3.3 Clay fraction analysis

As 'clay' can refer to grain size as well as mineralogy, this study uses the term clay fraction to define the fine-grained fraction of less than 2 µm including clay minerals but also other minerals such as quartz grains (Grim, 1942). The relative weight percentage of the clay fraction of homogenized sediment subsamples was measured on 33 samples from the P.U.C.H.F., 67 samples from Plassac and 41 samples from Richard. The clay-size fraction was detached from the sand grains using a sonicator probe. Samples were weighed in order to obtain the same dry mass of 5 g. They were then suspended in distilled (DI) water before being decarbonated using 20% acetic acid to remove the fine carbonate fraction, and the fine organic-matter fraction was also removed using 35% H2O2. After agitation, the suspension was allowed to rest for 1 hour 35 minutes. Then, the top 2 cm of the supernatant water (containing the clay grain-size particles) was sampled. The operation was repeated until the top 2 cm of the supernatant water was clear. The sampled fraction (< 2 µm) was

dried and weighed in order to calculate the weight percentage of the clay fraction in the sediment. It was expressed as a weight percentage of the sample (wt. %). Values obtained for the P.U.C.H.F. are underestimated because not all the denser and thicker authigenic clay minerals were included in this measure. Chlorite coatings and dickite crystals in intergranular space are greater than 10 µm in some samples (Saïag et al., 2016).

Composition of the clay fraction (< 2 µm) was then determined by X-ray diffraction analysis (XRD) with PANalytical X'Pert Pro (PANalytical, Almelo, The Netherlands) with a Cu anticathode (Kα1 1/4 1.540598, 45 kV; 40 mA) from 2 theta: 3–30° (step: 300 s and 0.0334°). Determination of clay mineral associations was based on the study of air-dried, ethylene-glycol saturated, and 550 °C-heated oriented powders (Brindley, 1961). Semi-quantitative estimations of smectite, illite, kaolinite and chlorite were made with Macdiff software based on the peak area of the ethylene-glycol diffractograms summed to 100%, the relative error for the peak area being ±5% (Petschick, 2001).

4. Results

4.1 Facies description and vertical facies succession

Six lithofacies were defined from core descriptions based on lithology, dominant sedimentary process and depositional context. Facies associations and their interpretations are described in detail in Table 1, with brief descriptions and possible interpretation in terms of depositional environment. Synthetic logs illustrating both vertical facies associations of the P.U.C.H.F. and the Holocene clastic sediment of the Gironde tidal bars are shown in Figure 3. Detailed facies descriptions and interpretations and the vertical facies associations are provided in appendix S1. A sedimentological log of part of the Petrel E core is chosen as a reference to illustrate the P.U.C.H.F. and the associated depositional facies (Fig. 4). The same

terminology was used to describe facies from the Gironde estuary and facies from the P.U.C.H.F. as similar facies are identifiable and comparable within both tidal settings (Table 1). Cores from well E are composed of tidal bars with similar sedimentary structures to those observed in the Gironde (Virolle et al., *in prep*). The bottom is made up of muddy deposits with the Fluid mud facies (F1). The Lower sand bar facies (facies F2) is composed of small tidal dunes with frequent and thick clayey sedimentary structures such as mud pebbles and clay drapes. Above, the middle part of tidal bars is composed by the Middle sand bar facies (F3), sand dominated, or by the Middle bar muddy facies (F4), mud-dominated. In the Gironde, facies (F3) within the Plassac tidal bar is richer in clayey sedimentary structures (mud pebbles and clay drapes) than the Richard tidal bar. Within the Gironde, these facies are capped by the Upper sand bar facies (F5), sand dominated. It can be rich in mud pebbles (F5a) with abundant mud pebbles on dune foresets (Plassac tidal bar), or on the contrary it can be poor in clays with rare clay drapes or mud pebbles (F5b, Richard tidal bar). The Tidal flat facies (F6), observed in the Plassac tidal bar, cap the underlying facies and consists of three types of bedding (flaser, wavy and lenticular) that are vertically stacked.

Comparisons between modern and ancient deposits indicate that at least five tidal bars are stacked within the P.U.C.H.F. well E (Fig. 4). Tidal bar thickness varies from 3.5 m to more than 7 m (not decompacted) within this formation. A synthetic vertical facies association can be reconstructed within this deeply buried sedimentary succession of the Petrel sub-basin (Fig. 4). Tidal bars from the Gironde consist of 8–10 m thick vertical successions (Fig. 3). The two vertical successions (Richard and Plassac tidal bars) display coarsening-upward facies sequences (Fig. 3).

For the entire clastic deposits under study, facies are typical of depositional environments ranging from outer estuary funnel (muddy central basin) to inner estuary funnel (bay-head

delta, Table 1 and Fig. 4).

4.2 Sand and sandstone petrography

Based on the study of 27 samples from the P.U.C.H.F. well E, the original feldspar content ranges from 16 to 33% and the present-day feldspar content ranges from 4 to 14% corresponding to an evolution from subarkose to quartzarenite during diagenesis (Fig. 5A). Samples from the Gironde estuary vary from litharenite to feldspathic litharenite (Fig. 5A).

Grain composition differs slightly between tidal bars from the P.U.C.H.F. and those from the Gironde estuary. On average, grain content (> 63 µm) represents *ca.* 76% of the total rock composition within the P.U.C.H.F. cores, while it represents *ca.* 67% and *ca.* 73% within the Plassac and Richard Gironde estuary tidal bars (Table 2).

For the Plassac tidal bar of the Gironde estuary, on average for 52 thin sections, samples are mostly composed of quartz (34%), feldspar (8%), lithics (16%), clay (30%) and porosity (14%) (Table 2, Fig. 5B-C). Samples vary from feldspathic litharenite to litharenite, grains are moderately well sorted overeall, and the mean grain size is about 228 µm (Table 2, Fig. 5A-C).

For the Richard tidal bar, sand grain composition varies slightly. This bar is mostly composed, on average for the 32 thin sections, of quartz (36%), feldspar (6%), lithics (15%), clay (24%) and porosity (14%) (Fig. 5D, Table 2). The main difference with the Plassac tidal bar is the non-negligible content of bioclast fragments (*ca.* 5%) in the Richard tidal bar (Fig. 5D). Samples belong mostly to the litharenite class as the proportion of carbonated lithics is higher than within the other tidal bars in the Gironde estuary (Table 2, Fig. 5A and D). Grains are mostly fine (average of 182 µm) and moderately sorted (Table 2). Detrital grains from

both tidal bars frequently have clay minerals attached to their surfaces forming detrital clay grain coats (Fig. 5B-D).

For the P.U.C.H.F., grains are, on average for 27 samples, mostly composed of quartz (66%), feldspar (present day ratio of about 7%), lithics (2%), clay fraction (5%), cement (14%) and porosity (10% for primary plus secondary porosities) (Table 2, Fig. 5E-G). It corresponds to subarkose to quartzarenite sandstones (Fig. 5A). Grains are globally fine, with a mean grain size *ca*. 150 µm, which is close to the Richard tidal bar. Grains are on average moderately to well sorted (Fig. 5E-G). Diagenetic features are observed such as feldspar dissolution, quartz overgrowth, pseudomatrix development or plastic deformation of micas squeezed between resistant quartz and framework grains (Fig. 5E-G).

4.3 Clay minerals within sand and sandstones

Clay fraction content varies between modern and buried deposits. On average, all facies included, it is very low within the P.U.C.H.F. (average of 5 wt% on 37 samples) while it is higher in the Gironde estuary tidal bars (average of 30 wt% on 71 samples at Plassac and 24 wt% on 42 samples at Richard; Table 2). Variations are found along the vertical facies associations of each deposit (Figs 4 and 7A). On average within the P.U.C.H.F., the Fluid mud facies (F1) displays the highest clay fraction content (8 wt% and 5 wt% in F1b and F1a respectively), while the others facies range between 2 and 4 wt% (Table 2, Figs 4 and 7A). Tidal bars from the Gironde estuary also have the highest clay fraction content within mud-rich facies (F1b, F2, F4 and F6) with clay fractions ranging from 25 to 58 wt% (Fig. 7A, Table 2).

Within the Gironde estuary tidal bars, clay mineral analysis by XRD allows us to identify four clay minerals (Figs 7B-E and 8A-B): (i) chlorite, characterized by diffraction peaks (001) at

14.10Å, (002) at 7.05Å, (003) at 4.73Å and (004) at 3.54Å; (ii) illite diffraction patterns show diffraction peaks (001) around 9.99Å, (002) at 4.99Å and (003) at 3.33Å; (iii) kaolinite displays diffraction peaks (001) at 7.16Å and (002) at 3.57Å; (iv) smectite is identifiable after ethylene-glycol saturation, with a diffraction peak (001) close to 17 Å.

Within the P.U.C.H.F., clay mineral composition differs with the presence of an illite-rich illite/smectite (I/S) mixed layer in all samples analysed by XRD (Fig. 8C). The EDX spectra under SEM indicate that the chlorites are Fe-rich within the P.U.C.H.F. The IR spectra of diagenetic kaolins are typical of dickite with shoulders at 3710 cm^{-1} and 3655 cm^{-1} (Beaufort et al., 1998; Saiag et al., 2016).

Chlorite has the highest surface area in XRD diffractograms and is the main clay mineral within the clay assemblage observed in the P.U.C.H.F. followed by the illite-rich I/S mixed layer (Figs 4 and 7; Table 2). Chlorite is observed in almost every sample in SEM within the P.U.C.H.F.

Within the Gironde estuary tidal bars, dominant detrital clay minerals within the clay fraction are smectite and illite, with more smectite in the inner estuary funnel (Plassac) and more illite in the outer estuary funnel (Richard; Fig. 7; Table 2).

4.4 Clay coating in sands and sandstones

Sand grains from the P.U.C.H.F. and from the Gironde estuary share the particularity of having clay minerals around their surfaces forming clay coatings (Figs 5B-G and 9). Of the total grain content measured within samples, *ca*. 25% at Plassac and 17% at Richard are coated (Figs 5B-D, 6D and 9A-D, Table 2). Within the P.U.C.H.F. well, grain content within samples is *ca*. 76% and *ca*. 67% of grains are coated (average of 26 samples; Table 2, Figs 5E-G, 6D and 9E-H).

Within the P.U.C.H.F., grain coating varies slightly within the different facies, ranging from 60% to 73%, for an average of 66% (Fig. 6D, Table 2). Clay coatings in the P.U.C.H.F. cover on average 61% of the outer sand perimeter (Table 2). Coat coverage (on the available surface as previously specified) is higher in facies F2 where *ca.* 71% of the available surface is coated on average, and lower in facies F1a (*ca.* 48 %), while it is roughly equivalent in the other facies (Table 2).

In the Plassac tidal bar, coated grain content ranges on average from 22% (F6) to 29% (F5a), while this content is lower in the Richard tidal bar, ranging from 14% (F5b) to 19% (F1b; Fig. 6D; Table 2). In facies F3, *ca.* 26% of grains in the Plassac tidal bar are coated while *ca*. 17% are coated in the Richard tidal bar. Coats cover on average 11% of grain surfaces in the Richard tidal bar and 19% in the Plassac tidal bar (Fig. 9A-D, Table 2). Coat coverage is low in facies F2 of the Richard tidal bar (*ca.* 5%), while it is higher in facies F2 of the Plassac tidal bar (*ca.* 25%, Table 2). In each modern and ancient deposit, no correlation is found between coated grain content and increasing depth or porosity variations.

Within the Gironde estuary, coatings are detritic and are essentially composed of detrital clay minerals (smectite and illite essentially) associated with other components such as carbonates, pyrite, diatoms or silt-sized quartz (Figs 5B-D and 9A-D). The Richard tidal bar has the particularity of displaying coated carbonated components such as gastropods, bivalves or echinoderms (Figs 5D and 9D). Within the P.U.C.H.F., coatings are composed of well-crystallized Fe-rich chlorites that are mostly oriented perpendicular to the grain surface (Fig. 9E-H). Thickness varies from 2 to 10 µm approximately. Coatings are mostly continuous around sand grains (Fig. 9E-F).

As observed by Saiag et al. (2016), densely packed clay mineral aggregates composed of chlorite are sometimes located beneath or close to the well-crystallized coating with more euhedral and more widely spaced chlorite crystals (Fig. 10).

Finally, similar coating textures can be observed in both tidal settings with clays that drape the surface of sand grains (Fig. 9A, 9E and 9F), or with aggregates at the surface of framework grains (Fig. 9B-D and 9G-H). In the Gironde estuary, other textures can be observed as bridges between detritic grains or even ridged textures (Fig. 9B).

5. Discussion

5.1 Influence of detrital materials on chloritization

In low-temperature geological systems such as burial diagenesis, chlorite is more likely to arise from chloritization processes through mixed-layer mineral series than from direct precipitation from solution (Beaufort et al., 2015 and references therein). The formation of chlorite from the transformation of a clay-mineral precursor through a series of intermediate mixed-layer minerals is promoted as it requires low activation energy and is kinetically more likely (Putnis, 1992). This mean that the diagenetic chlorites observed in deeply buried sandstone reservoirs such as the P.U.C.H.F. are derived from specific clay precursors (Pagel et al., 2014; Saïag et al., 2016). Moreover, depending on the geochemical conditions, chloritization does not involve the transformation of just one mineral precursor via a single reaction mechanism (Aagard et al., 2000; Worden & Morad, 2003; Beaufort et al., 2015). Several reaction paths including several clay precursors lead to the formation of chlorite during burial (Worden and Morad, 2003).

Serpentine-like minerals such as berthierine and odinite are the most common clay precursors specified in the chloritization process of diagenetic Fe-chlorite (Worden and

Morad, 2003; Gould et al., 2010; Beaufort et al., 2015). Berthierine is an Fe-rich phyllosilicate that is formed from the interactions of the most reactive detrital Al-Fe minerals with sedimentary solutions under reducing conditions and/or from bioturbation with the ingestion of freshly deposited sediments by macro-organisms (Velde, 1985; Peyaud and Worden., 2007). It can also be formed during early burial (eodiagenesis) from the transformation of odinite or other reactive Al-bearing clay minerals (such as smectite) as long as ferrous iron is available in solution (Fig. 10, Pe-Piper et al., 2008; Morad et al., 2010). Then, berthierine can be transformed into Fe-rich chlorite such as chamosite in a temperature range of 40–120°C (Fig. 10, Beaufort et al., 2015).

In the Gironde, the detrital clay minerals composing the clay fraction are illite, smectite, chlorite and kaolinite (Jouanneau and Latouche, 1981; Virolle et al., 2019). These clay minerals forming detrital clay grain coats could be the pre-requisite sedimentary material that is essential for chlorite-precursor formation (Fig. 10).

Densely-packed clay mineral aggregates observed in the P.U.C.H.F., just beneath or close to the well-crystallized Fe-rich chlorite coating suggest that those aggregates might be the relics of initial detrital clay coats (Fig. 11). These aggregates might be the remnants from transformation of detrital clay grain coats or eogenetic smectite into berthierine if Fe^{2+} was available in solution, and after burial into well-ordered chlorite-smectite mixed layers and finally to Fe-rich chlorite (Fig. 10). These aggregates may also reveal the transformation of detrital kaolinite into berthierine as long as ferrous iron is available during eogenesis before forming Fe-rich chlorite through a dissolution and recrystallization process during burial (Fig. 10, Morad et al., 2000, Beaufort et al., 2015). Kaolinite is also transformed into dickite during burial. Besides, the absence of coatings on grain sutures suggests that the Fe-rich chlorite crystallization occurs after mechanical compaction of the sediment (Saïag et al., 2016).

Finally, formation of Fe-rich clay minerals requires labile Fe (Gould et al., 2010). Alteration of Mg and Fe-rich materials within the Gironde such as volcanic lithic, biotite and/or oxides and hydroxides (such as goethite or ferrihydrite) may release Fe^{2+} and Mg^{2+} which are then available for the chlorite formation process during diagenesis (Morad et al., 2000; McKinley et al., 2003). Moreover, dissolution of detrital clay minerals (such as smectite) mediated by microorganisms may release iron and silica into the surrounding pore waters (Vorhies and Gaines., 2009; Fang et al., 2017). This release of iron within ground water could improve the subsequent precipitation of clay minerals (such as berthierine) that may act as the precursors to Fe-rich chlorite leading to the chloritization process in estuarine sandstones. Therefore, the detrital minerals and detrital clay grain coats observed in the Gironde estuary could initiate the generation of Fe-rich chlorite during burial.

5.2 Tidal bar vertical facies succession

Tidal bars observed within P.U.C.H.F. and within the modern Gironde estuary can be quite similar in thickness despite the erosion and compaction that occurred in the ancient deposits (Fig. 3). In general, tidal bar dimensions are on the scale of estuary dimensions, in particular in width and depth (Leuven et al., 2016). It is likely, then, that the local estuary depth in the P.U.C.H.F. was similar to the depth of the Gironde estuary.

Each tidal bar from modern and ancient deposits presents a global coarsening-upward sequence (Figs 3 and 4). In the P.U.C.H.F. well, the vertical association is composed of several tidal bars stacked one on top of the other. A total of five tidal bars can be identified in well E (Fig. 4). Each displays similarities with the modern tidal bars as they exhibit sedimentary structures of tidal environments: (1) bidirectional cross-strata, (2) reactivation surfaces and (3) tidal bundles with clay drapes and sometimes mud-pebbles (Figs 3 and 4, Table 1).

Comparisons with the Gironde deposits show that facies deposited near the bottom of the tidal bar (facies F1-F2) are mud-rich and display many clayey sedimentary structures (thick clay drapes, mud pebbles or fluid mud layers) that will affect reservoir qualities (Figs 3 and 4, Table 1). Above, facies (F3), (F5a) and (F5b) are sandier but still with some clay drapes and mud pebbles (Fig. 4). In addition to muddy facies at the bottom of tidal bars, large clay baffles are also settled within the facies associations of tidal bars in P.U.C.H.F. deposits, as observed in tidal bar 2, and in the Gironde tidal bars (facies F4; Figs 3 and 4; Féniès and Tastet, 1998; Chaumillon et al., 2013).

Besides, facies F4 could originate from similar processes in both of the modern and ancient tidal settings under study. Tidal bar 2 from the P.U.C.H.F. displays a similar arrangement to the Richard tidal bar in the Gironde with the superimposition of two sand units displaying cross-bedded sand facies (F3), separated by a muddy layer exhibiting muddy-sand tidal rhythmite facies (F4; Figs 3 and 4). As observed in another Gironde tidal bar, facies (F4) in the Richard tidal bar corresponds to a long period of low river discharge, causing sand-starvation and allowing the decantation of many fine particles (Féniès and Tastet, 1998). The same process may have occurred in the Permian deposits for the settlement of this facies in tidal bar 2.

The depositional environment of the P.U.C.H.F. might therefore have been very similar to the Gironde estuary in terms of hydrodynamic conditions and turbidity, producing a very similar vertical facies succession within the tidal bars. The top of the Petrel tidal bars, normally marked by tidal flat or tidal marsh facies, may have been eroded before the deposition of the following tidal bar. This is why they are not observed.

5.3 Tidal bar location within the palaeo-estuary

Differentiating between tidal bars deposited in the inner estuary funnel and those deposited in the outer part can prove difficult. Comparison with a modern estuary can provide some clues. First of all, in terms of grain size. The mean grain sizes measured in P.U.C.H.F. tidal bars are almost similar to those measured in the Richard tidal bar within the Gironde (*ca*. 150 µm in Petrel and 182 µm in the Richard tidal bar; Table 2, Fig. 6C). Tidal bars from the bay-head delta, such as the Plassac tidal bar, tend to be slightly coarser (*ca.* 228 µm; Table 2, Fig. 6C). Within the clay assemblages of modern tidal bars, smectite is probably more common in the Plassac tidal bar (with coarser grains) than in the Richard tidal bar, which is richer in illite, while chlorite and kaolinite are relatively homogeneous in both tidal bars (Fig. 7, Table 2). This distribution is similar in other modern estuaries such as the Ravenglass estuary where illite is most abundant in the fine-grained sediments of the inner estuary and mud from the central basin (Griffiths et al., 2018).

Besides, each tidal bar is heterolithic, but to various degrees (Fig. 3). In the Gironde, tidal bars from the bay-head delta (such as Plassac) seem more heterolithic, with more clayey heterogeneities at various scales, from large clay layers such as facies F1a and F4, to the higher concentration of clay drapes and mud pebbles as are found within facies F3 or F5a (Fig. 12, Table 1). The clay fraction content is also higher in the Plassac than the Richard tidal bar (Table 2, Fig. 7A), and facies (F3) and (F5a) from the Plassac tidal bar have more and thicker clay drapes and mud pebbles than (F3) and (F5b) from the Richard tidal bar. In the Gironde, this can be explained by the TMZ position that is more regularly centred in the vicinity of the Plassac than the Richard tidal bar (Allen et al., 1977; Doxaran et al., 2008). In the P.U.C.H.F., tidal bars 3 to 5 display less clayey sedimentary structures than tidal bars 1 and 2.

All these clues combined may suggest the tidal bars in the P.U.C.H.F. vertical succession were mainly deposited in an outer (tidal bars 3 to 5) rather than an inner (tidal bars 1 and 2) estuary funnel (Fig. 4).

5.4 Origin of unstratified mud deposits

Fluid muds are a relatively new criterion for identifying tidal conditions within distributary channel deposits (Longhitano et al., 2012). A fluid mud deposit is defined as a bottom-hugging mobile subaqueous body composed of fine-grained sediment with a concentration of tens to hundreds $g.l^{-1}$ (Parker and Kirby, 1982; Jalón-Rojas et al., 2015). They can be recognized in the rock record as centimetre- to decimetre-thick unbioturbated and unlaminated mud layers, and in the distributary channels they occur in the lower parts of the channel fill (Longhitano et al., 2012). Fluid mud appears to be especially common in areas beneath the Turbidity Maximum Zone (TMZ) as within the Gironde estuary (Parker and Kirby, 1982; Wright et al., 1988; Uncles et al., 2006; Ichaso and Dalrymple, 2009; Sottolichio et al., 2011). Fluid mud deposits and thick clay drapes observed within the P.U.C.H.F. well may indicate that the estuary was mud-rich with a well-developed TMZ as observed in the Gironde estuary (Figs 1 and 12). All these muddy layers, as well as facies F4, will act as large clay baffles affecting connectivity between sandy reservoir units (Fig. 12).

5.5 Multi-scale reservoirs characterization

Reservoir characterization requires a multi-scale approach. On a large scale (x100 m), heterogeneities must be considered, and notably clay layers that will act as baffles (Wood, 2004; Massart, 2014). Comparisons with modern estuarine deposits may allow us to determine how clay baffles can affect fluid flow within sandy reservoir units. Since facies (F1)

and (F4) are continuous over several tens to hundreds of metres in the Gironde estuary deposits, it is possible that these same facies within the P.U.C.H.F. deposits constitute large-scale discontinuities (Figs 3 and 12).

On smaller scales within the P.U.C.H.F., the best reservoir properties are observed in facies F3 with notably five samples that stand out (14A, 17A, 18A, 19B and 51B; Fig. 13A). These samples also correspond to a coated grain content of more than 60% (Fig. 13B), a clay fraction content that ranges from 3 wt% to 10 wt% (Fig. 13C) and chlorite content among this clay fraction mostly exceeding 1% (Fig. 13D). Despite a certain percentage of coated grains, the thickness of the coating can affect the variations in porosity and permeability for the same percentage of coated grains (thick coatings block pore spaces), just as a clay content that is too low or too high can affect these parameters (forming pore filling or allowing quartz overgrowth).

Although well E deposits display abundant and sometimes thick clayey sedimentary structures (such as fluid mud or clay drapes), the clay fraction (< 2 µm) within samples is very low (Table 2). It can be partly explained by diagenetic events with dissolution and recrystallization of detrital clay minerals but also by particle transport due to fluid flow during burial. Therefore, the final content of the fraction lower than 2 µm will be lower than the initial content.

As coarser-grained sandstones have a smaller surface area relative to bulk volume and thus require less clay content to achieve full surface coverage, the optimum grain coat coverage to preserve porosity might be influenced by mean grain size (Bloch et al. 2002). Bloch et al. (2002) report that a relatively minor amount of clay content (even as little as 1–2% of the rock volume) can form extensive coats on individual sand grains. Other authors such as

Pittman et al. (1992) suggest an optimum range of 4–7% sediment volume as in clays for the Berea Sandstone and 5–12% in the Tuscaloosa Formation.

Sandy facies (F3 and F5b) from tidal bars located in the outer estuary funnel of the Gironde, such as the Richard tidal bar, display fewer clayey sedimentary structures (clay drapes and mud pebbles) than the tidal bars located in the inner estuary funnel, such as the Plassac tidal bar (facies F5a; Figs 7 and 12, Table 2). The latter may experience pseudomatrix formation during eodiagenesis owing to pseudoplastic deformation and compaction of ductile grains between rigid grains (Morad et al., 2010). Besides, samples from the Richard tidal bar have, on average, a lower coat coverage (11%), a lower coated grain (17%) and a lower clay fraction (24 wt%) content than the Plassac tidal bar (25% of coated grain, 19% of coat coverage and clay fraction of 30 wt%, Figs 6 and 7, Table 2). However, it could be sufficient to form thin and continuous clay coating during burial, whereas in the Plassac tidal bar, too many and more developed coatings associated with a high clay fraction content can partially obstruct porosity and permeability during diagenesis.

In the Gironde, facies F3 and F5b deposited in the outer estuary funnel might therefore be the best reservoir units if preserved after burial (Fig. 12, Table 2).

Therefore, taking into account petrographic observations and facies descriptions in both modern and ancient tidal settings, better reservoir properties within an estuarine depositional environment might be preferentially located in tidal bars deposited in the outer estuary funnel than in tidal bars deposited in the inner estuary funnel. Sandy facies from the Middle sand bar facies (F3) to the Upper sand bar facies (F5b) with clay content of 20–25 wt% maximum, a coated grain of 15–20% and coat coverage of about 10% could be the ideal initial conditions for reservoir formation after burial (Figs 3 and 12).

5.6 Tidal bar sequence in a retrogradational sequence

Within the P.U.C.H.F., inter-well scale correlations can be made from gamma-ray and core descriptions (Kloss et al., 2004; Robinson and McInerney, 2003). Tidal sand bars facies that have been observed in the upper part of the Cape Hay Formation are the sandstone reservoir units targeted (Fig. 14). The Upper Cape Hay Formation within the Petrel sub-basin was deposited in shallow-marine to fluvial environments with a basin opening towards the north-northwest (Bhatia et al., 1984, Robinson and McInerney, 2003, Figs 1 and 14).

Differentiating between deposits laid down in the inner or outer estuary funnel can help to explain the stratigraphic evolution of the study area. Within the P.U.C.H.F. well, the transition from tidal bar 2 to tidal bar 4 may record a shift from tidal bars that belong to an inner part of a mud-rich palaeo-estuary to a more external area subject to the influence of higher tidal currents and probably of waves (Figs 4 and 12). It might therefore record the transgression period that occurred at this period with outer estuarine tidal bars that might overlie muddier inner estuarine tidal bars (Fig. 14).

Facies F3 has good petrographic properties in terms of coated grain content, coat coverage and porosity preservation (Figs 3, 6, 7 and 13, Table 2). Samples with better reservoir properties are located at the top of the transgressive cycle (Figs 3, 13 and 14). Other examples can be found around the world displaying well-preserved reservoir qualities within transgressive cycles and linked to chlorite coatings as within the Lower to Mid-Jurassic series of the Halten Banken Area (Norwegian Sea; Lafont et al., 2001). Besides, Morad et al. (2010) show that eogenetic grain coatings composed of berthierine, odinite and smectite are mostly formed in the Transgressive Systems Tract (TST) and early Highstand Systems Tract (HST) in deltaic and estuarine sandstones. These coatings can be transformed into ferrous chlorite during mesodiagenesis helping preservation of good sandstone reservoir properties.

In the Gironde, the highest concentration of smectite is found in the inner estuary tidal bars, but the latter are also associated with the highest clay fraction content that can obstruct pore throats (Fig. 7, Table 2).

Genetic stratigraphic sequence cyclicity (second- through fifth-order) might be considered when comparing modern and ancient deposits. In the Gironde, the TST comprises the bulk of the incised valley fill and forms a landward-thinning wedge of tidal-estuarine sands and muds (Allen and Posamentier, 1993). The HST, initiated at about 4000 BP, forms a seaward-prograding, tide-dominated estuary head delta that has been gradually filling the estuary since the post-Holocene stillstand (Allen and Posamentier, 1993). In buried and ancient analogues, the same time scales are not necessarily observable, notably because of erosion. The trend observed in the P.U.C.H.F. belongs to a third-order transgressive period (5–10 Ma) and only the transgressive trend can now be seen.

However, integrating all the results, the best reservoir facies are located at the top of transgressive sequence, preferentially in outer estuarine funnel tidal bars in sand rich facies located from the Middle sand bar facies (F3) to the Upper sand bar facies (F5b) if preserved, which is not the case for the P.U.C.H.F. concerning the facies (F5b), with fewer multi-scale clay heterogeneities and optimal petrographic and mineralogical characteristics (Figs 3, 12 and 13, Table 2).

Conclusions

Comparisons between estuarine sands cored within two tidal bars from the Gironde estuary and sandstones from P.U.C.H.F. show that sediments of P.U.C.H.F. were deposited in a palaeo-estuary very similar to the present-day Gironde estuary.

Vertical facies associations of tidal bars are very similar with many common facies between ancient and modern deposits such as a muddy bottom, deposited near the estuary channel floor, overlain by sandier facies indicative of an increase in hydrodynamic conditions. Extensive clay layers may be deposited in the middle sand bar areas owing to hydrodynamic variations or to specific processes (e.g. lateral accretion processes).

Vertical facies associations and sedimentary structures observed in tidal bars from the P.U.C.H.F might have been deposited in a mud-rich palaeo-estuary with a well-developed TMZ as indicated by fluid mud deposits and clay drape thickness.

Facies comparisons indicate that facies from the middle to the upper sand bar areas deposited in the outer estuarine tidal bars may be the best reservoir facies. They have a mean grain size about 150–180 μm with fewer and thinner clayey sedimentary structures than are observed in the inner estuary tidal bars.

Detrital clay grain coats are observed in the modern Gironde tidal bars. About 20% of grains are coated and coatings display various textures as aggregates. Fe-rich chlorite coatings are observed in every sample of the Upper Cape Hay Formation (Petrel). The absence of Fe-rich clay coating between grains suggests that crystallization occurred after mechanical compaction. Observations of densely-packed aggregates within the P.U.C.H.F., similar to detrital clay coats observed in the modern Gironde estuary, suggest that transformation of detrital clay might be at the origin of well-crystallized Fe-rich chlorite during burial. In the Gironde, detrital clay minerals within detrital clay grain coats can initiate chloritization in sandstone that is done in at least two steps. The first occurs during eogenesis, with very shallow burial, where detrital minerals such as kaolinite or smectite evolve into berthierine if Fe^{2+} is available in the pore water. Then, this mineral may serve as a precursor to Fe-rich chlorite transformation during burial. The transition from detrital clays into Fe-rich chlorite

during eogenesis and burial diagenesis through berthierine should be more thoroughly explored. Several processes can dissolve detrital minerals and release Fe, such as microbial activity, promoting berthierine formation and then Fe-rich chlorite crystallization.

Sandy facies forming sand bars during transgressive cycles, and mostly those deposited at the top of the sequence before the settlement of the clay seal, might be good candidates for finding clay coatings and well-preserved sandstone reservoir qualities. From petrographic observations of sand bar facies in the Gironde estuary, sandy facies with a maximum clay content of 20–25 wt%, associated with coated grain content of 15–20% and coat coverage of about 10% could be the ideal initial conditions for reservoir formation after burial. In ancient estuarine sandstones, good reservoir qualities must be sought vertically in the last sequences of third-order cycles below the clay seal and horizontally in sediments deposited in outer estuary funnels.

Acknowledgements

This work is the result of collaborative project No. P04980 CLAYCOAT 'CLAY COATing in shallow marine clastic deposits to improve reservoir quality prediction' between University Paris-Sud, Bordeaux INP, University of Bordeaux Montaigne, University of Poitiers and Neptune Energy. This study has benefitted greatly from Neptune Energy funding. The authors would also like to thank Serge Miska (GEOPS) for assistance with XRD analysis. We are grateful to Valérie Godard (GEOPS) for high-quality thin sections.

Figure captions

Figure 1: (A) Location of the Petrel sub-basin and simplified geological map modified after Earl (2004). (B) Permian lithostratigraphy of the Bonaparte Basin and reservoir arrangement, modified from Bhatia et al. (1984); Formation nomenclature after Gorter (1998). (C) Proposed palaeo-environmental reconstruction for the Petrel sub-basin during the Permian.
2-column fitting image

Figure 2: (A) Gironde estuary location with simplified sedimentological map along the estuary. Locations of tidal bars cored in B and C. (B) Side-scan sonar picture of the "u-shaped" inner estuarine Plassac tidal bar and core location within the eastern spit. (C) The elongated outer estuarine Richard tidal bar and core locations.
2-column fitting image

Figure 3: Vertical facies associations with synthetic logs of the Gironde tidal bars (Plassac and Richard) and of the Permian Upper Cape Hay Formation deposits. Facies are illustrated with core pictures and interpretations.
2-column fitting image

Figure 4: Sedimentological log of the Permian Upper Cape Hay Formation deposits and evolution with depth of: the depositional area within the palaeo-estuary, gamma-ray, porosity (separating primary and secondary), permeability, mean grain size, clay assemblage and clay fraction content.
2-column fitting image

Figure 5: (A) QFL ternary diagrams with samples from the Gironde tidal bars (left) and from the Permian Upper Cape Hay Formation (right) with distinction of initial and present feldspar content. (B) Microphotograph of framework grains from the Plassac tidal bar (white arrows indicate clay coatings around sand grains); (C) Microphotograph of framework grains from the Plassac tidal bar with sand grains in contact with a clay laminae; (D) Microphotograph of framework grains from the Richard tidal bar with clay coating carbonates; (E) Microphotograph of framework grains from Petrel with quartz grains, quartz overgrowth, and primary and secondary porosity; (F) Microphotograph of framework grains from Petrel with micas deformed by compaction; (G) Microphotograph of framework grains from the Petrel deposits with a clay matrix between sand grains.
Qz.= Quartz; Fd= Feldspars; Li= Lithic grains; Ca= Carbonates; B= Biotite; Mu= Muscovite; Qz.O= Quartz Overgrowth; DFd= Dissolved feldspars
2-column fitting image

Figure 6: (A) Porosity, (B) Sorting, (C) Mean grain size and (D) Coated grain content as a function of sedimentary facies and tidal settings. Porosity for Petrel samples includes both primary and secondary porosity.
2-column fitting image

Figure 7: (A) Clay fraction content within the total rock volume, (B) Detrital smectite, (C) Detrital and authigenic chlorite, (D) Detrital illite and authigenic illite-rich illite-smectite (I/S) mixed layer and (E) Detrital kaolinite and authigenic dickite content, all as a function of sedimentary facies and tidal setting.
2-column fitting image

Figure 8: X-Ray diffractograms showing clay minerals identifiable within (A) the Plassac tidal bar, (B) the Richard tidal bar and (C) the Permian Upper Cape Hay Formation. The

terminology N corresponds to air dried samples, EG for ethylene-glycol saturation and CH for heating at 550 °C. Ethylene-glycol diffractograms were used for semi-quantifications.
2-column fitting image

Figure 9: Picture compilation showing (A-D) detrital and (E-H) authigenic clay coatings within each tidal setting. (A) Microphotograph from the Plassac tidal bar with coated sand grains forming essentially bridges between grains; (B-C) Scanning Electron Microscopy (SEM) pictures from the Plassac and Richard tidal bars showing detrital clay grain coats forming aggregates at the surface of detrital grains; (D) Microphotograph from the Richard tidal bar showing coated framework grains including carbonates (purple arrows); (E-F) Microphotographs from the Petrel deposits illustrating authigenic clay coats around sand grains preserving porosity; (G-H) SEM pictures of Fe-rich chlorite coatings around quartz grain. White arrows indicate coatings; Abbreviations mean: Qz= Quartz; Li= Lithic grains; Fd= Feldspars.
2-column fitting image

Figure 10: Schematic illustration of possible evolutions of detrital clay minerals during burial diagenesis. I/S= Illite-smectite mixed layer; C/B= chlorite-berthierine mixed layer.
2-column fitting image

Figure 11: SEM picture from the Permian Upper Cape Hay Formation showing densely packed aggregates linked to thin and continuous clay coating. These aggregates might be the relic of detrital clay grain coats transformed during burial.
1.5 to 2-column fitting image

Figure 12: Synthetic diagram based on the comparison with a modern tidal setting showing retrogradational tidal bars in a muddy palaeo-estuary. Comparisons with modern analogues indicate that tidal bars may have large-scale heterogeneities affecting reservoir properties. The vertical facies association and clayey sedimentary structure content (mud pebbles or clay drapes) depend on the location within the inner (orange tidal bars) or outer (yellow tidal bars) part of the estuary. This will affect the petrographic properties with potentially more or less clay pore filling despite clay coatings. The best reservoir qualities can be found in the sandier outer estuarine tidal bars. Sandy facies with a maximum clay content of 20–25 wt%, associated with coated grain content of 15–20% and coat coverage of about 10% could provide the ideal initial conditions for reservoir formation after burial.
2-column fitting image

Figure 13: Porosity-permeability relation in samples from the Permian Upper Cape Hay Formation as a function of (A) facies, (B) coated grain content, (C) clay fraction content and (D) chlorite content within samples.
2-column fitting image

Figure 14: Simplified inter-well correlations throughout the Petrel sub-basin with tidal bar evolution seaward (North/North-East) to landward (South/South-West), modified after Kloss et al. (2004). Petrographic observations are replaced so as to determine locations of the best reservoirs properties.
2-column fitting image

Table 1: Table of facies recognized in this study

Table 2: Data table for each facies from the Gironde estuary tidal bars and from the Permian Upper Cape Hay Formation tidal bars sampled in this study

References

Aagaard, P., Jahren, J.S., Harstad, A.O., Nilsen, O., Ramm, M., 2000. Formation of grain-coating chlorite in sandstones. Laboratory synthesized vs. natural occurrences. Clay Miner. 35, 261.

Aase, N.E., Bjorkum, P.A., Nadeau, P.H., 1996. The effect of grain-coating microquartz on preservation of reservoir porosity. AAPG Bulletin 80 (10), 1654-1673.

Allen, G.P., 1973. Etude des processus sédimentaires dans l'estuaire de la Gironde. Institut de géologie du bassin d'Aquitaine, 5.

Allen, G.P., Castaing, P., 1973. Suspended sediment transport from the Gironde estuary (France) onto the adjacent continental shelf. Mar. Geol. (14), 47-53.

Allen, G.P., 1991. Sedimentary processes and facies in the Gironde estuary: a recent model for macrotidal estuarine systems. In: Clastic Tidal Sedimentology (Eds R.A. Rahmani, D.G. Smith, G.E. Reinson and B.A. Zaitlan), Mem. Canadian Soc. Petrol. Geol. 16, 29-39.

Allen, G.P. and Posamentier, H.W., 1993. Sequence stratigraphy and facies model of an incised valley fill: The Gironde Estuary, France. SEPM J. Sediment. Res. 63 (3), 378-391.

Allen, G.P., Sauzay, G., Castaing, P., Jouanneau, J.M., 1977. Transport and deposition of suspended sediment in the Gironde Estuary, France. Estuar. Process. 2, 63-81.

Allen, J.R.L., Rae, J.E., 1988. Vertical salt-marsh accretion since the Roman period in the Severn Estuary, southwest Britain. Mar. Geol. 83, 225-235.

Aschoff, J.L., Olariu, C., Steel, R.J., 2018. Recognition and significance of bayhead delta deposits in the rock record: A comparison of modern and ancient systems. Sedimentology 65, 62-95.

Beaufort, D., Baronnet, A., Lanson, B., Meunier, A., 1997. Corrensite: A single phase or a mixed-layer phyllosilicate in the saponite-to-chlorite conversion series? A case study of Sancerre-Couy deep drill hole (France). American Mineralogist 82, 109-124.

Beaufort, D., Rigault, C., Billon, S., Billault, V., Inoue, A., Inoue, S., Patrier, P., 2015. Chlorite and chloritization processes through mixed-layer mineral series in low-temperature geological systems: A review. Clay Minerals 50, 497-523.

Bhatia, M.R., Thomas, M., Boirie, J.M., 1984. Depositional framework and diagenesis of the late Permian gas reservoirs of the Bonaparte Basin. APPEA J. 24, 299-313.

Billault, V., Beaufort, D., Baronnet, A. and Lacharpagne, J.C., 2003. A nanopetrographic and textural study of grain-coating chlorites in sandstone reservoirs. Clay Minerals 38, 315-328.

Bjørlykke, K., 1979. Discussion. Cementation of sandstones. J. Sediment. Petrol. 49, 1358-1359.

Bjørlykke, K., Egeberg, P.K., 1993. Quartz cementation in sedimentary basins. AAPG Bull. Am. Assoc. Petrol. Geol. (United States) 77 (9), 1538-1548.

Bloch, S., Lander, R.H., Bonnell, L., 2002. Anomalously high porosity and permeability in deeply buried sandstone reservoirs: Origin and predictability. AAPG Bull. 86, 301-328.

Boyd, R., Dalrymple, R.W., Zaitlin, B.A., 2006. Estuarine and incised-valley facies models. SEPM Spec. Publ. 84, 171-235.

Bottig, M., Gier, S., Jilg, W., 2017. Artificially induced clay mineral authigenesis in an underground gas storage field, North Alpine Foreland Basin, Austria. AAPG Bulletin 101 (6),

789-806.
Brindley, G.W., 1961. The X-ray identification and crystal structures of clay minerals. Mineralogical Society, Clay Minerals Group, 242-296.
Brown, L.F., 1993. Seismic and sequence stratigraphy: Its current status and growing role in exploration and development (course notes): New Orleans Geological Society. Short Course.
Chang, H.K., Mackenzie, F.T., Schoonmaker, J., 1986. Comparisons between the diagenesis of dioctahedral and trioctahedral smectite, Brazilian offshore basins. Clays and Clay Minerals 34 (4), 407-423.
Coughenour, C.L., Archer, A.W., Lacovara, K.J., 2009. Tides, tidalites, and secular changes in the Earth–Moon system. Earth-Sci. Rev. 97, 59-79.
Dalrymple, R.W., Rhodes, R.N., 1995. Estuarine dunes and bars. Dev. Sedimentol. 53, 359-422.
Daneshvar, E., Worden, R.H., 2018. Feldspar alteration and Fe minerals: Origin, distribution and implications for sandstone reservoir quality in estuarine sediments. In P.J. Armitage, A.R. Butcher, J.M. Churchill, A.E. Csoma, C. Hollis, R.H. Lander, . . . R.H. Worden (Eds.), Reservoir Quality of Clastic and Carbonate Rocks: Analysis, Modelling and Prediction. Special Publication 435. London: Geological Society. 129-139
Davies, J.L., 1964. A morphogenic approach to world shorelines. Zeitschrift fur Geomorphologie 8, 127-142.
Del Negro, R., Desaubliaux, G., 2010. Core description and sedimentary model Petrel field, Bonaparte basin, Australia (Confidential No. GDF-Suez).
Dolson, J., Muller, D., Evetts, M., Stein, J.A., 1991. Regional paleotopographic trends and production, Muddy Sandstone (Lower Cretaceous), Central and Northern Rocky Mountains. AAPG Bull. 75, 409-435.
Dowey, P.J., Worden, R.H., Utley, J., Hodgson, D.M., 2017. Sedimentary controls on modern sand grain coat formation. Sediment. Geol. 353, 46-63.
Doxaran, D., Froidefond, J.M., Castaing, P., Babin, M., 2009. Dynamics of the turbidity maximum zone in a macrotidal estuary (the Gironde, France): Observations from field and MODIS satellite data. Estuar. Coast. Shelf Sci. 81, 321-332.
Earl, K.L., 2004. Bonaparte Basin Petroleum Systems. Geosci. Aust. GEOCAT 61365.
Fenies, H., De Resseguier, A., Tastet, J.P., 1999. Intertidal clay-drape couplets (Gironde estuary, France). Sedimentology 46, 1-15.
Fenies, H., Tastet, J.P., 1998. Facies and architecture of an estuarine tidal bar (the Trompeloup bar, Gironde Estuary, SW France). Mar. Geol. 150, 149-169.
Folk, R.L., 1980. Petrology of Sedimentary Rocks. Hemphill Publishing Company.
Gorter, J.D., 1998. Revised Upper Permian stratigraphy of the Bonaparte Basin. In: Purcell, P.G., Purcell, R.R. (Eds). The Sedimentary Basins of Western Australia 2, Proceedings of The Petroleum Exploration Society of Australia Symposium, Perth, 213-228.
Gould, K., Pe-Piper, G., Piper; J.W., 2010. Relationship of diagenetic chlorite rims to depositional facies in Lower Cretaceous reservoir sandstones of the Scotian Basin. Sedimentology 57, 587-610.
Griffiths, J., Worden, R.H., Wooldridge, L.J., Utley, J.E.P., Duller, R.A., 2018. Detrital clay coats, clay minerals, and pyrite: a modern shallow-core analogue for ancient and deeply buried estuarine sandstones. Journal of Sedimentary Research 88 (10), 1205-1237.
Griffiths, J., Worden, R.H., Wooldridge, L.J., Utley, J.E.P., Duller, R.A., Edge, R.L., 2019. Estuarine clay mineral distribution: Modern analogue for ancient sandstone reservoir quality prediction. Sedimentology, in press.

Grim, R.E., 1942. Modern concepts of clay materials. J. Geol. 50, 225-275.
Haile, B.G., Hellevang, H., Aagaard, P., Jahren, J., 2015. Experimental nucleation and growth of smectite and chlorite coatings on clean feldspar and quartz grain surfaces. Mar. Pet. Geol. 68, 664-674.
Harris, P.T., Collins, M.B., 1985. Bedform distributions and sediment transport paths in the Bristol Channel and Severn Estuary, UK. Mar. Geol. 62, 153-166.
Heald, M.T., Larese, R.E., 1974. Influence of coatings on quartz cementation. J. Sediment. Res. 44, 1269-1274.
Herringshaw, L.G., McIlroy, L.G., 2013. Bioinfiltration: Irrigation-driven transport of clay particles through bioturbated sediments. J. Sediment. Res. 83, 443-450.
Hillier, S., 1994. Pore-lining chlorites in siliciclastic reservoir sandstones: Electron microprobe, SEM and XRD data, and implications for their origin. Clay Minerals 29 (4), 665-680.
Ichaso, A.A., Dalrymple, R.W., 2009. Tide-and wave-generated fluid mud deposits in the Tilje Formation (Jurassic), offshore Norway. Geology 37 (6), 539-542.
Jouanneau, J.M., Latouche, C., 1981. The Gironde Estuary. Eds Fuchtbauer, H., Lisitzyn, A.P., Milliman, J.D., Seibold, D. In: Contribution to Sedimentology, Stuttgart, 1981, 115p.
Klein, G.D., 1998. Clastic tidalites—A partial retrospective view. SEPM Spec. Publ. Tidalites: Processes and Product, 5-14.
Khalifa, M., Morad, S., 2012, Impact of structural setting on diagenesis of fluvial and tidal sandstones: The Bahi Formation, Upper Cretaceous, NW Sirt Basin, North Central Libya. Marine and Petroleum Geology 38, 211-231.
Kloss, O., Wood, G., Benson, J., Lang, S., Bann, K., Kassan, L., 2004. A revised depositional model for the Cape Hay Formation, Petrel Field, northern Australia. Timor Sea Pet. Geosci. Proc. Timor Sea Symp. Darwin North. Territ. 19-20 Northern Territory Geological Survey, 503-518.
Lafont, F., Lacharpagne, J.J., Euvreard, B., Lejay, A., Lawrence, D. 2001. Porosity preservation in deeply buried coated sandstones of the Norwegian Sea: Understanding early diagenetic processes in a high-resolution sequence stratigraphic framework. AAPG Annual Meeting 2001, Denver, AAPG Bulletin 85.
Lander, R.H., Larese, R.E., Bonnell, L.M., 2008. Toward more accurate quartz cement models: the importance of euhedral versus noneuhedral growth rates. American Association of Petroleum Geologists, Bulletin 92, 1537-1563.
Larsonneur, C., 1975. Tidal deposits, Mont Saint-Michel Bay, France, in: Tidal Deposits. Springer, 21-30.
Lericolais, G., Fémes, H., Tastet, J.-P., Berné, S., 1998. Reconnaissance par stratigraphie sismique haute résolution de la paléovallée de la Gironde sur le plateau continental. Comptes Rendus Académie Sci.-Ser. IIA-Earth Planet. Sci. 326, 701-708.
Lericolais, G., Berné, S., Féniès, H., 2001. Seaward pinching out and internal stratigraphy of the Gironde incised valley on the shelf (Bay of Biscay). Mar. Geol. 175, 183-197.
Leuven, J.R.F.W., Kleinhans, M.G., Weisscher, S.A.H., Van der Vegt, M., 2016. Tidal sand bar dimensions and shapes in estuaries. Earth Sciences Reviews 161, 204-223.
Longhitano, S.G., Mellere, D., Steel, R.J., Ainsworth, R.B., 2012. Tidal depositional systems in the rock record: A review and new insights. Sediment. Geol. 279, 2-22.
Mamadou, M.M., Cathelineau, M., Bourdelle, F., Boiron, F.C., Elmaleh, A., Brouand, M., 2016. Hot fluid flows around a major fault identified by paleothermometric studies (Tim Mersoï basin, Niger). JSR 86, 914-928.

Martinius, A.W., Ringrose, P.S., Brostrom, C., Elfenbein, C., Naess, A., Ringas, J.E., 2005. Reservoir challenges of heterolithic tidal sandstone reservoirs in the Halten Terrace, mid-Norway. Pet. Geosci. 11, 3-16.
Massart, B.Y.G., 2014. Improved characterisation and modelling of heterolithic tidal sandstone reservoirs. Imperial College London, London.
McBride, E.F., 1989. Quartz cement in sandstones: A review. Earth-Science Rev. 26, 69-112.
McKinley, J.M., Worden, R.H., Ruffell, A.H., 2003. Smectite in sandstones: A review of the controls on occurrence and behavior during diagenesis. Int. Assoc. Sedimentol. Spec. Publ. 34, 109-128.
Morad, S., Al-Ramadan, K., Ketzer, J.M., De Ros, L.F., 2010. The impact of diagenesis on the heterogeneity of sandstone reservoirs: A review of the role of depositional facies and sequence stratigraphy. AAPG Bulletin 94 (8), 1267-1309.
Musial, G., Reynaud, J.Y., Gingras, M.K., Féniès, H., Labourdette, R., Parize, O., 2012. Subsurface and outcrop characterization of large tidally influenced point bars of the Cretaceous McMurray Formation (Alberta, Canada). Sediment. Geol. 279, 156-172.
Pagel, M., Barbarand, J., Beaufort, D., Gautheron, C., Pironon, J., (2014). Bassins sédimentaires-les marqueurs de leur histoire thermique. SGF 228p.
Parker, W., Kirby, R., 1982. Sources and transport patterns of sediment in the inner Bristol Channel and Severn Estuary. In: Severn Barrage: Proceedings of a Symposium Organized by the Institution of Civil Engineers, Presented at the Severn Barrage: Proceedings of a symposium organized by the Institution of Civil Engineers, London, 181-194.
Petschick, R. (2001) Macdiff- a programme for analysis and display of X-ray powder diffractogrammes on Apple Macintosh platforms. Available at: http://www.geologie.unifrankfurt.de/staff/Homepages/Petschick/MacDiff/MacDiffInfoE.html.
Peyraud, J.B., Worden, R.H., 2007. The bioclay factory: Digestion as a clay-generating process. In: Proceedings of the 12th Water-Rock Interaction Conference (T.D. Bullen and X. Wang. editors). Taylor and Francis, Kunming, China, 533-536.
Pittman, E.D., Larese, R.E., Heald, M.T., 1992. Clay coats: Occurrence and relevance to preservation of porosity in sandstones. Origin, diagenesis, and petrophysics of clay minerals in sandstones. SEPM (Society for Sedimentary Geology), 241-255.
Putnis, A., 1992. An Introduction to Mineral Sciences. Cambridge, Cambridge University Press, 457 p.
Robert L. Folk, Ward, W., 1957. Brazos river bar: A study in the significance of grain size parameters. J. Sediment. Res. 27, 3-26.
Robinson, P., Mcinerney, K., 2003. Permo-Triassic reservoir fairways of the Petrel Sub-basin, Timor Sea, in: Timor Sea Petroleum Geoscience. Proceedings of the Timor Sea Symposium, Darwin, Northern Territory. 19-20.
Roduit, N., 2007. JMicroVision: un logiciel d'analyse d'images pétrographiques polyvalent. Section des Sciences de la Terre, Université de Genève, Genève, 129p.
Saïag, J., Brigaud, B., Portier, É., Desaubliaux, G., Bucherie, A., Miska, S., Pagel, M., 2016. Sedimentological control on the diagenesis and reservoir quality of tidal sandstones of the Upper Cape Hay Formation (Permian, Bonaparte Basin, Australia). Mar. Pet. Geol. 77, 597-624.
Seebeck, H., Tenthorey, E., Consoli, C., Nicol, A., 2015. Polygonal faulting and seal integrity in the Bonaparte Basin, Australia. Marine and Petroleum Geology. 60, 120-135.
Sottolichio, A., Castaing, P., Etcheber, H., Maneux, E., Schmeltz, M., Schmidt, S., 2011.

Observations of suspended sediment dynamics in a highly turbid macrotidal estuary, derived from continuous monitoring. J. Coast. Res. Special Issue, 1579-1583.
Steel, R.J., Plink-Bjorklund, P., Aschoff, J., 2012. Tidal Deposits of the Campanian Western Interior Seaway, Wyoming, Utah and Colorado, USA. In: Davis, R.A., Dalrymple, R.W. (Eds.), Principles of Tidal Sedimentology. Springer Netherlands, Dordrecht, 437-471.
Storvoll, V., Bjørlykke, K., Karlsen, D., Saigal, G. (Eds.), 2002. Porosity preservation in reservoir sandstones due to grain-coating illite: A study of the Jurassic Garn Formation from the Kristin and Lavrans fields, offshore Mid-Norway. Marine and Petroleum Geology 19 (6), 767-781.
Uncles, R.J., Stephens, J.A., Law, D.J., 2006. Turbidity maximum in the macrotidal, highly turbid Humber Estuary, UK: Flocs, fluid mud, stationary suspensions and tidal bores. Estuarine, Coastal and Shelf Science 67, 30-52.
Van Wagoner, J., Mitchum, R., Campion, K., Rahmanian, V., 1990. Methods in Siliciclastic Sequence Stratigraphy in Well Logs, Cores, and Outcrops. Concepts for High-Resolution Correlation of Time and Facies, Associations of Petroleum Geologist. AAPG Methods in Exploration Series, Tulsa Oklahoma.
Velde, B., 1985. Clay Minerals: A Physico-Chemical Explanation of Their Occurrence. Elsevier Amsterdam, v. 40, 427 p.
Virolle, M., Brigaud, B., Bourillot, R., Féniès, H., Portier, E., Duteil, T., Nouet, J., Patrier, P., Beaufort, D., 2018. Detrital clay grain coats in estuarine clastic deposits: Origin and spatial distribution within a modern sedimentary system, the Gironde Estuary (south-west France). Sedimentology, 66(3), 859-894.
Vorhies, J.S., Gaines, R.R., 2009. Microbial dissolution of clay minerals as a source of iron and silica in marine sediments. Nature Geoscience 2, 221-225.
Walderhaug, O., 1996. Kinetic modeling of quartz cementation and porosity loss in deeply buried sandstone reservoirs. AAPG Bull. 80 (5), 731-745.
Walker, T.R., 1976. Diagenetic Origin of Continental Red Beds. The Continental Permian in Central, West, and South Europe. Springer, 240-282.
Walker, T.R., Waugh, B., Grone, A.J., 1978. Diagenesis in first-cycle desert alluvium of Cenozoic age, southwestern United States and northwestern Mexico. Geol. Soc. Am. Bull. 89, 19-32.
Wilson, M.D., Pittman, E.D., 1977. Authigenic clays in sandstones; recognition and influence on reservoir properties and paleoenvironmental analysis. J. Sediment. Res. 47, 3-31.
Wood, L.J., 2004. Predicting tidal sand reservoir architecture using data from modern and ancient depositional systems. In: Integration of outcrop and modern analogs in reservoir modeling. AAPG Memoir 80, 45-66.
Wooldridge, L.J., Worden, R.H., Griffiths, J., Utley, J.E.P., 2017a. Clay-coated sand grains In petroleum reservoirs: Understanding their distribution via a modern analogue. J. Sediment. Res. 87, 338-352.
Wooldridge, L.J., Worden, R.H., Griffiths, J., Thompson, A., Chung, P., 2017b. Biofilm origin of clay-coated sand grains. Geology 45 (10), 875-878.
Wooldridge, L.J., Worden, R.H., Griffiths, J., Utley, J.E.P., Thompson, A., 2018. The origin of clay-coated sand grains and sediment heterogeneity in tidal flats. Sedimentary Geology 373, 191-209.
Wooldridge, L.J., Worden, R.H., Griffiths, J., Utley, J.E., 2019. Clay coat diversity in marginal marine sediments. Sedimentology.
Worden, R.H., Morad, S. (Eds.), 2003. Clay mineral cements in sandstones, Special

publication number 34 of the International Association of Sedimentologists. Blackwell Science Ltd., Oxford, UK.
Wright, L.D., Wiseman, W.J., Bornhold, B.D., Prior, D.B., Suhayda, J.N., Keller, G.H., Yang, Z.S., Fan, Y.B., 1988. Marine dispersal and deposition of Yellow River silts by gravity-driven underflows. Nature 332 (6165), 629.
Zhixin, W., Guanghui, Z., Lin'an, P., Wenlian, T., 2012. An oil and gas resource reassessment of the Bonaparte Basin, northwest shelf of Australia. Bull. Can. Pet. Geol. 60, 218-226.

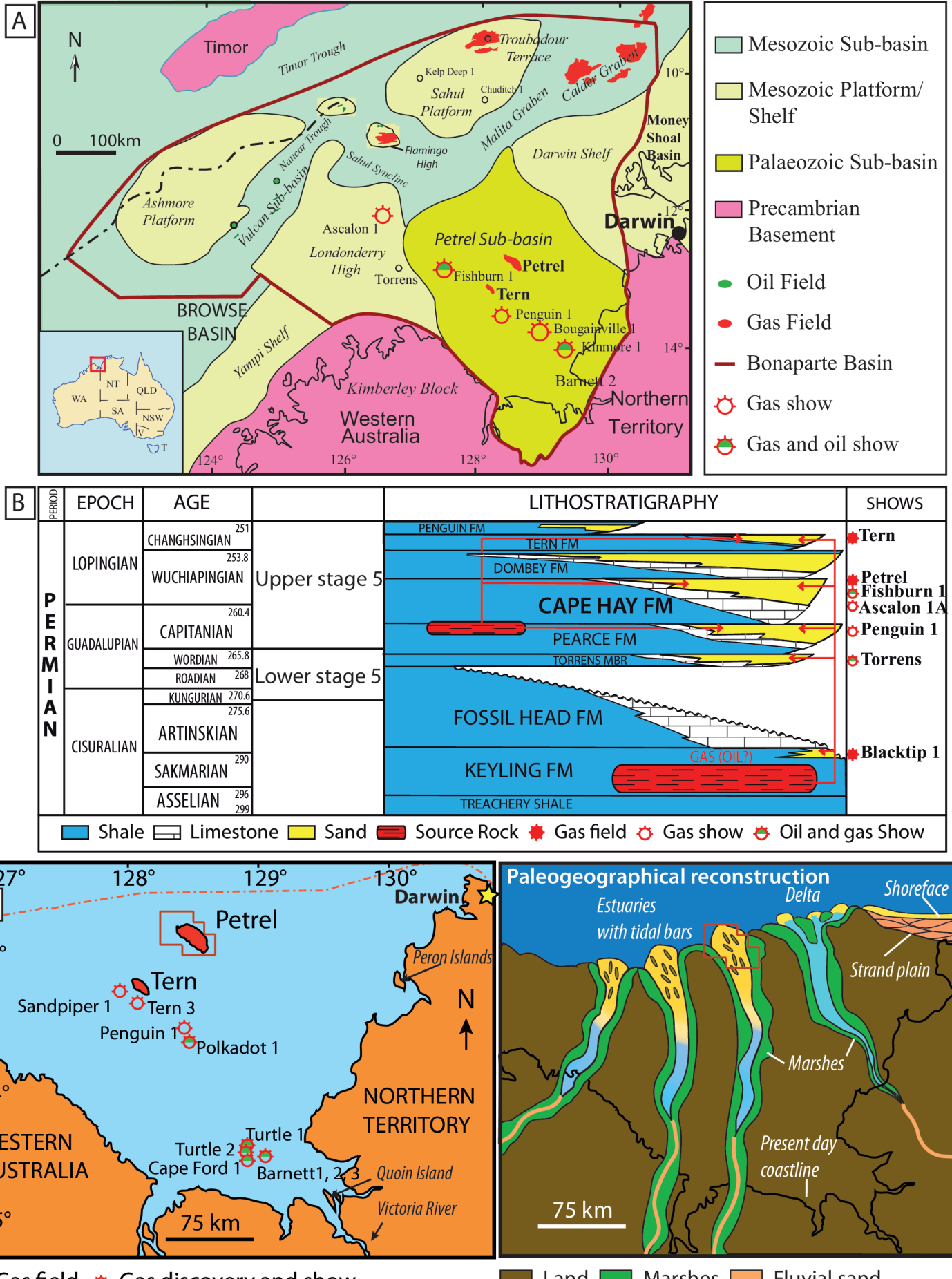
A
N
0 100km
Timor
Timor Trough
Troubadour Terrace
Kelp Deep 1
Sahul Platform
Chuditch 1
Calder Graben
Malita Graben
Money Shoal Basin
Darwin Shelf
Flamingo High
Sahul Syncline
Nancar Trough
Vulcan Sub-basin
Ashmore Platform
Ascalon 1
Londonderry High
Torrens
Petrel Sub-basin
Fishburn 1
Petrel
Tern
Penguin 1
Bougainville 1
Kinmore 1
Barnett 2
Darwin
BROWSE BASIN
Yampi Shelf
Kimberley Block
Western Australia
Northern Territory
10°
12°
14°
124°
126°
128°
130°
NT
QLD
WA
SA
NSW
Mesozoic Sub-basin
Mesozoic Platform/ Shelf
Palaeozoic Sub-basin
Precambrian Basement
Oil Field
Gas Field
Bonaparte Basin
Gas show
Gas and oil show
B
PERIOD
EPOCH
AGE
LITHOSTRATIGRAPHY
SHOWS
PERMIAN
LOPINGIAN
GUADALUPIAN
CISURALIAN
CHANGHSINGIAN 251
WUCHIAPINGIAN 253.8
CAPITANIAN 260.4
WORDIAN 265.8
ROADIAN 268
KUNGURIAN 270.6
ARTINSKIAN 275.6
SAKMARIAN 290
ASSELIAN 296 299
Upper stage 5
Lower stage 5
PENGUIN FM
TERN FM
DOMBEY FM
CAPE HAY FM
PEARCE FM
TORRENS MBR
FOSSIL HEAD FM
KEYLING FM
GAS (OIL?)
TREACHERY SHALE
Tern
Petrel
Fishburn 1
Ascalon 1A
Penguin 1
Torrens
Blacktip 1
Shale
Limestone
Sand
Source Rock
Gas field
Gas show
Oil and gas Show
C
127°
128°
129°
130°
Darwin
Petrel
13°
Peron Islands
Tern
Sandpiper 1
Tern 3
Penguin 1
Polkadot 1
N
14°
NORTHERN TERRITORY
WESTERN AUSTRALIA
Turtle 1
Turtle 2
Cape Ford 1
Barnett1, 2, 3
Quoin Island
Victoria River
15°
75 km
Paleogeographical reconstruction
Estuaries with tidal bars
Delta
Shoreface
Strand plain
Marshes
N
Present day coastline
75 km
Gas field
Gas discovery and show
Oil discovery with gas show
Land
Marshes
Fluvial sand
Muddy basin
Sand
Marine marls/clays

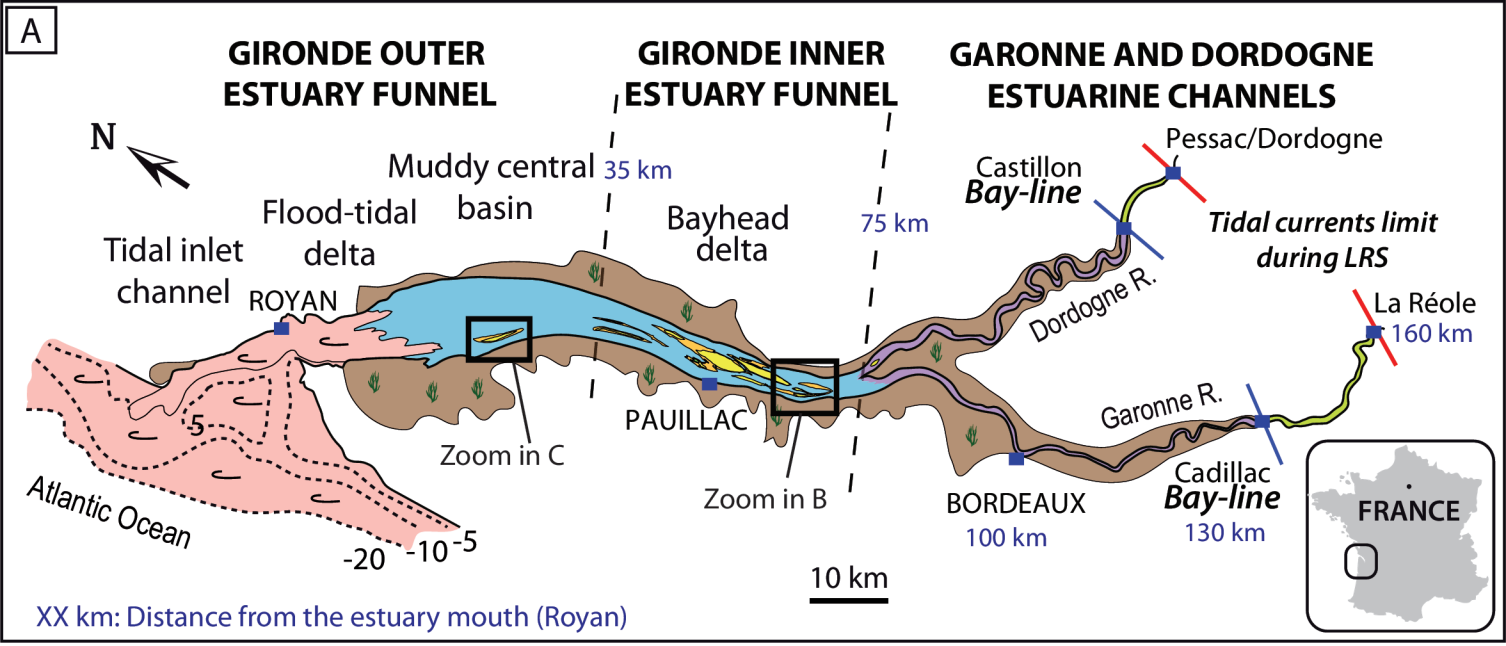

Legend A:

- Fluvial-estuarine transition point bars
- Estuarine heterolithic point bars
- Estuarine mud
- Tidal sand bars (bathymetry 0 m)
- Tidal sand bars (bathymetry -2 m)
- Estuary mouth and shelf sand
- Bathymetric lines

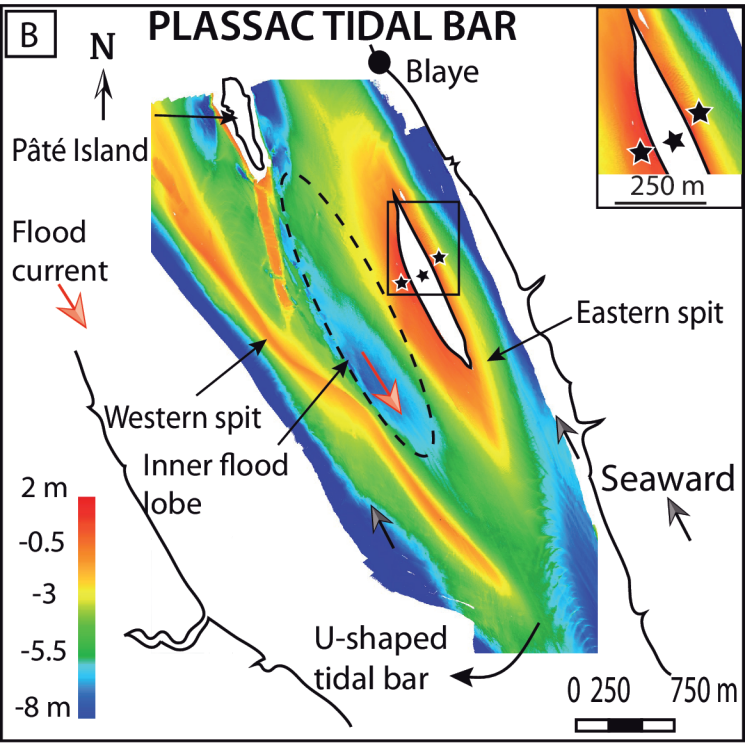

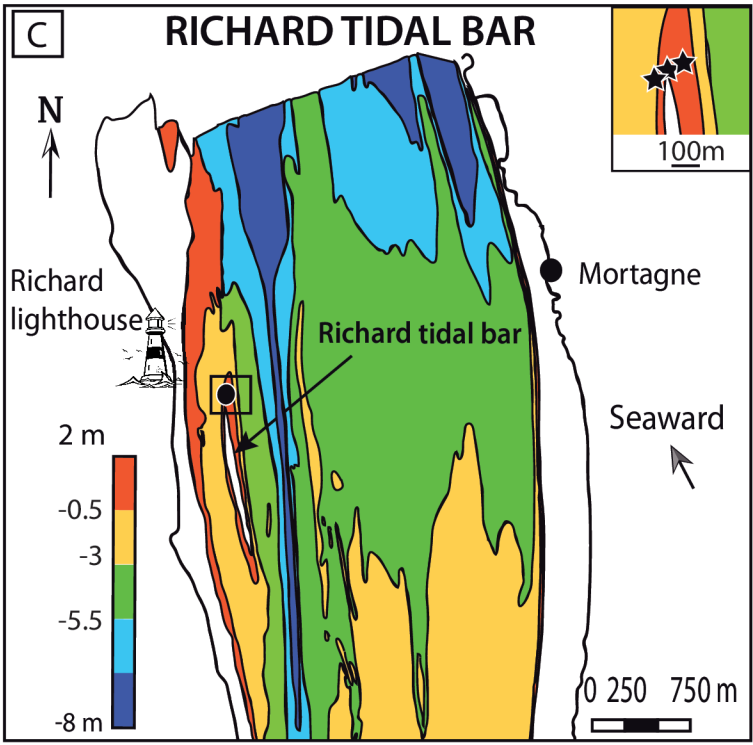

Legend B-C:

★ Cores transect in each tidal bar

Vertical facies associations of modern and ancient estuarine deposits

SYNTHETIC LOG: VERTICAL FACIES ASSOCIATION OF THE PLASSAC TIDAL BAR

Location: Gironde estuary
France
Inner estuary funnel
Average height: 10 meters

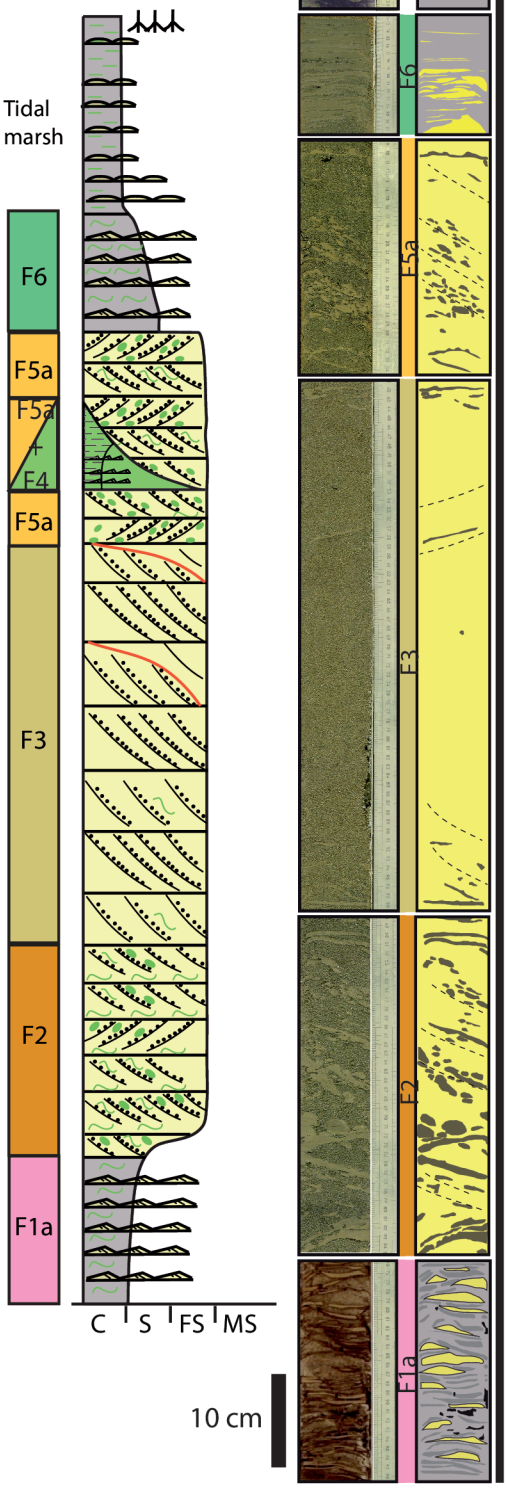

SYNTHETIC LOG: VERTICAL FACIES ASSOCIATION OF THE PETREL TIDAL BAR

Location: Bonaparte Basin,
Australia
Average height
of tidal bars: 6 meters
At least, 5 tidal bars stacked
the one on the others

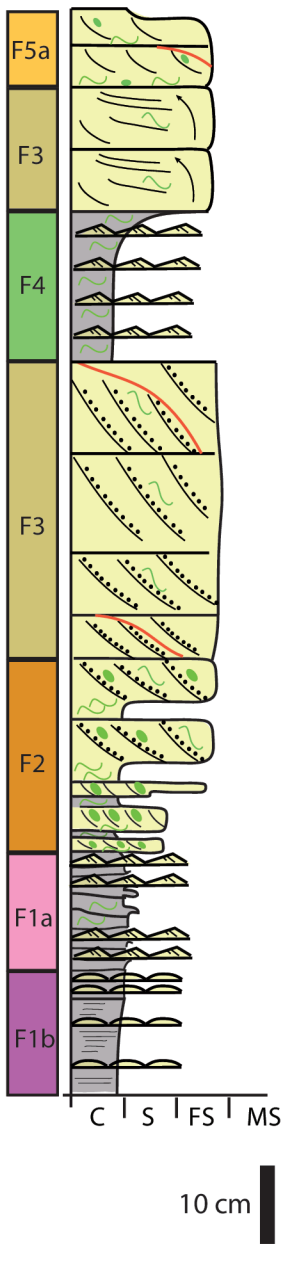

SYNTHETIC LOG: VERTICAL FACIES ASSOCIATION OF THE RICHARD TIDAL BAR

Location: Gironde estuary
France
Outer estuary funnel
Average height: 9 meters

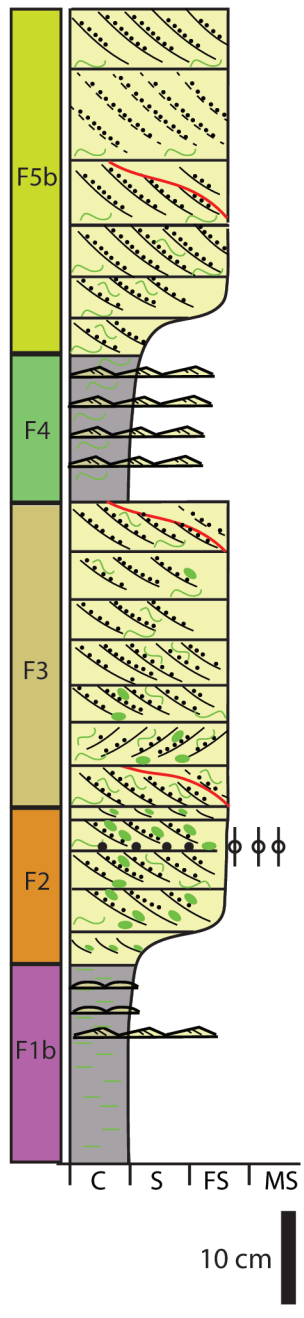

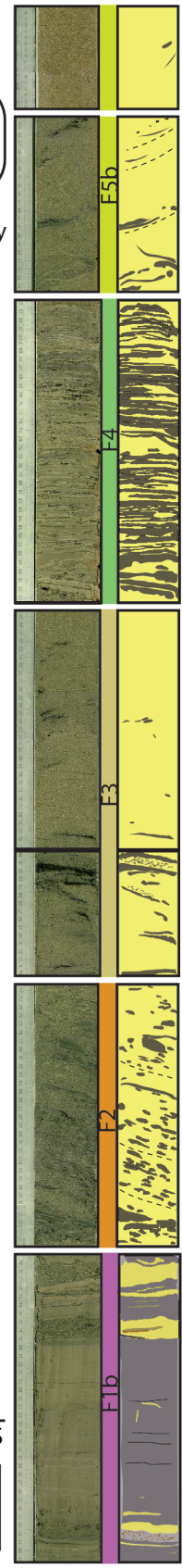

Clay; Silt; Fine Sand; Medium Sand

Amalgamated slack-water clay drapes with sandy linsens

Dunes with reactivation surfaces

Reed roots

Amalgamated slack-water clay drapes with sandy ripples

Dunes with clay drapes and mud pebbles

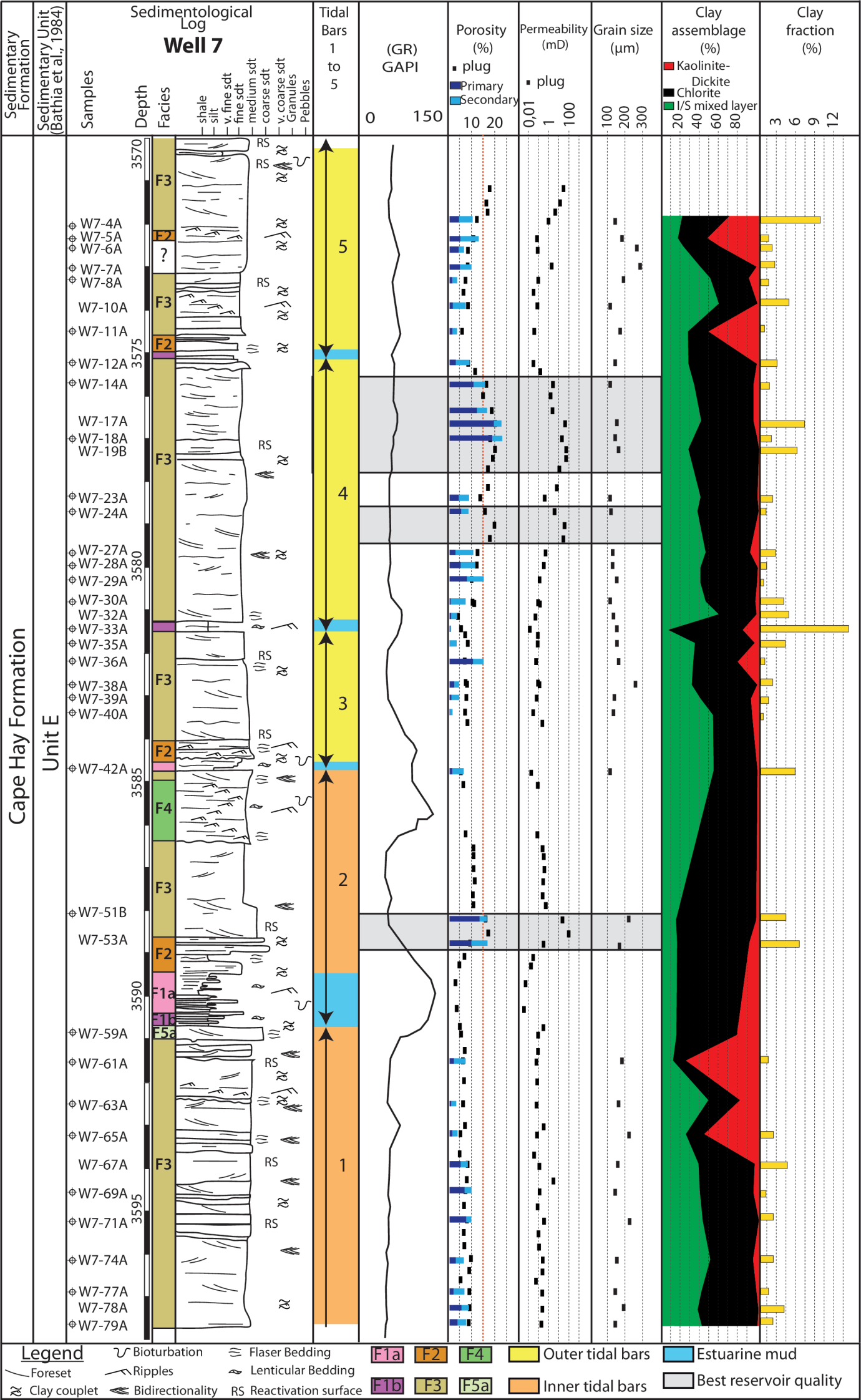
Sedimentary Formation
Sedimentary Unit (Bathia et al., 1984)
Sedimentological Log
Well 7
Samples
Depth
Facies
shale
silt
v. fine sdt
fine sdt
medium sdt
coarse sdt
v. coarse sdt
Granules
Pebbles
Tidal Bars 1 to 5
(GR) GAPI
0
150
Porosity (%)
plug
Primary
Secondary
10 20
Permeability (mD)
plug
0,01
1
100
Grain size (µm)
100
200
300
Clay assemblage (%)
Kaolinite-Dickite
Chlorite
I/S mixed layer
20 40 60 80
Clay fraction (%)
3 6 9 12
Cape Hay Formation
Unit E
3570
3575
3580
3585
3590
3595
F3
F2
?
F4
F1a
F1b
F5a
RS
W7-4A
W7-5A
W7-6A
W7-7A
W7-8A
W7-10A
W7-11A
W7-12A
W7-14A
W7-17A
W7-18A
W7-19B
W7-23A
W7-24A
W7-27A
W7-28A
W7-29A
W7-30A
W7-32A
W7-33A
W7-35A
W7-36A
W7-38A
W7-39A
W7-40A
W7-42A
W7-51B
W7-53A
W7-59A
W7-61A
W7-63A
W7-65A
W7-67A
W7-69A
W7-71A
W7-74A
W7-77A
W7-78A
W7-79A
5
4
3
2
1
Legend
Foreset
Clay couplet
Bioturbation
Ripples
Bidirectionality
Flaser Bedding
Lenticular Bedding
RS Reactivation surface
F1a
F1b
F2
F3
F4
F5a
Outer tidal bars
Inner tidal bars
Estuarine mud
Best reservoir quality

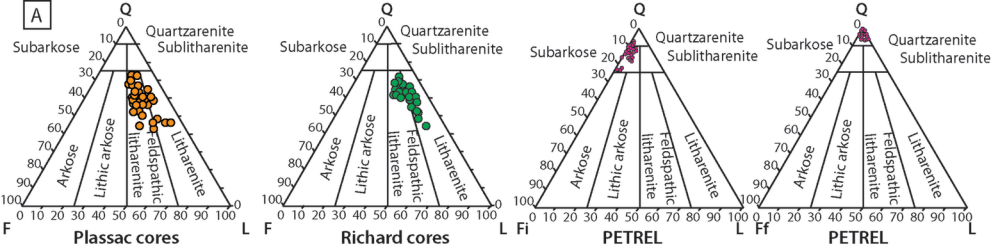
A
Q
Quartzarenite
Subarkose
Sublitharenite
Arkose
Lithic arkose
litharenite
Feldspathic
Lithatenite
F
L
Plassac cores
Richard cores
Fi
Ff
PETREL

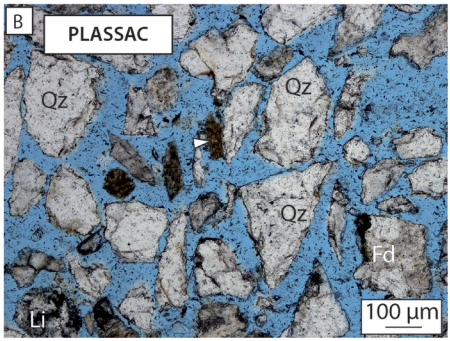
B
PLASSAC
Qz
Fd
Li
100 µm

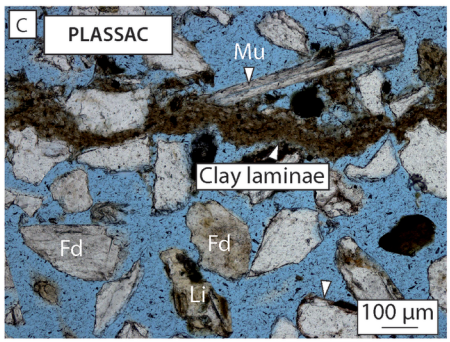
C
PLASSAC
Mu
Clay laminae
Fd
Li
100 µm

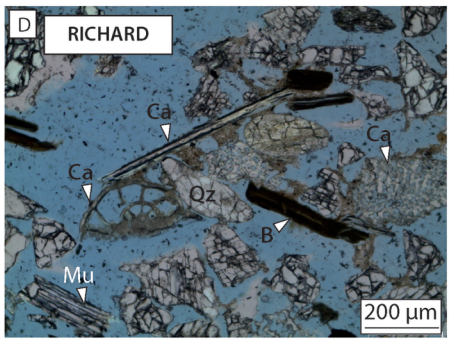
D
RICHARD
Ca
Qz
B
Mu
200 µm

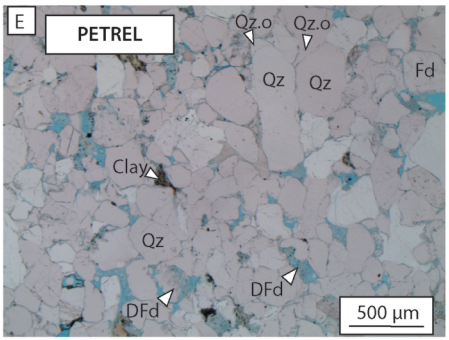
E
PETREL
Qz.o
Qz
Fd
Clay
DFd
500 µm

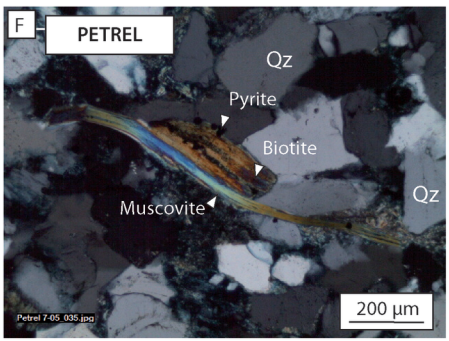
F
PETREL
Qz
Pyrite
Biotite
Muscovite
200 µm

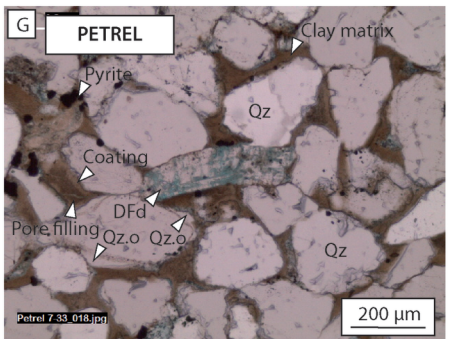
G
PETREL
Clay matrix
Pyrite
Qz
Coating
DFd
Pore filling
Qz.o
200 µm

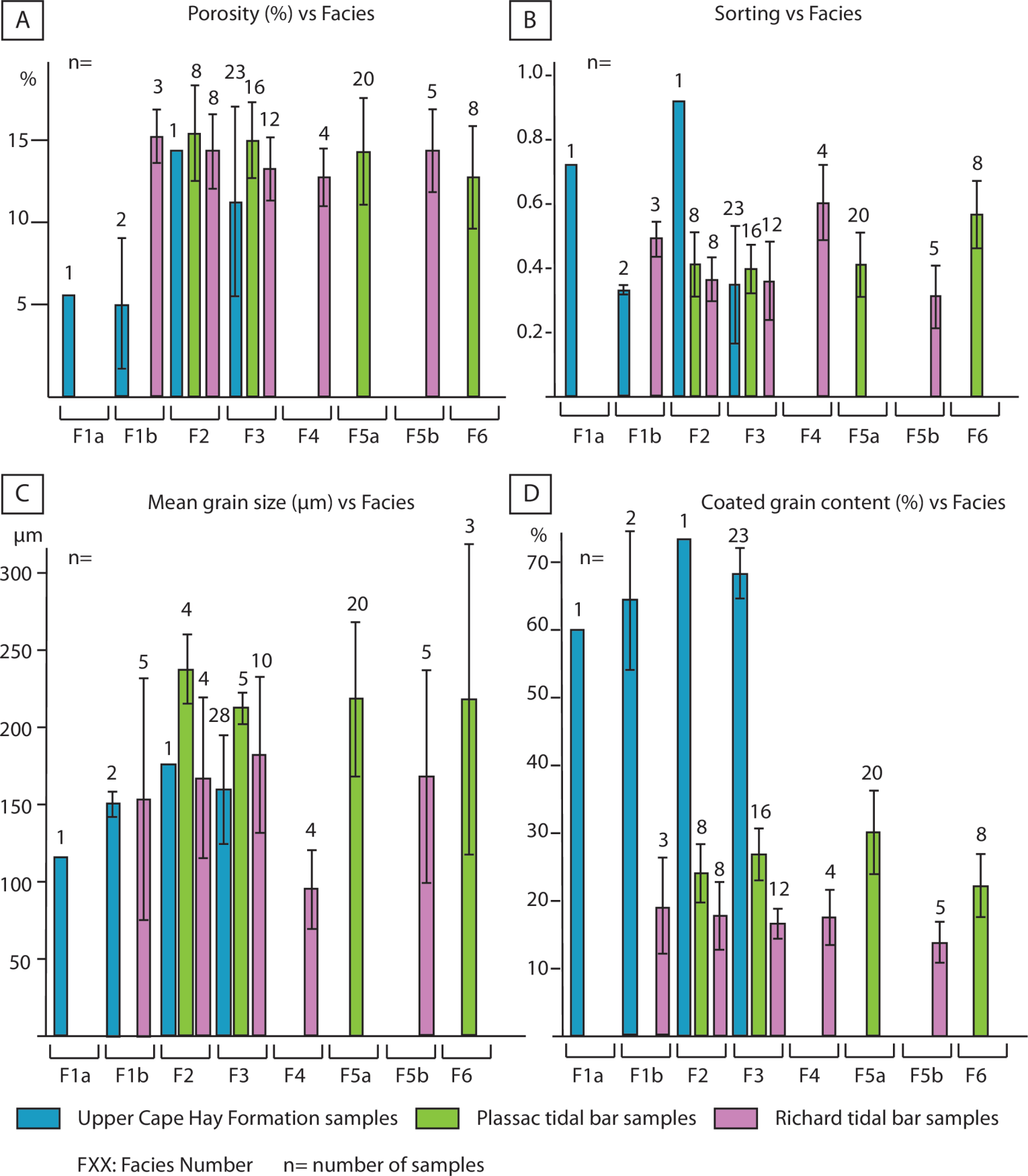
A
Porosity (%) vs Facies
%
n=
B
Sorting vs Facies
C
Mean grain size (µm) vs Facies
µm
D
Coated grain content (%) vs Facies
F1a
F1b
F2
F3
F4
F5a
F5b
F6
Upper Cape Hay Formation samples
Plassac tidal bar samples
Richard tidal bar samples
FXX: Facies Number
n= number of samples

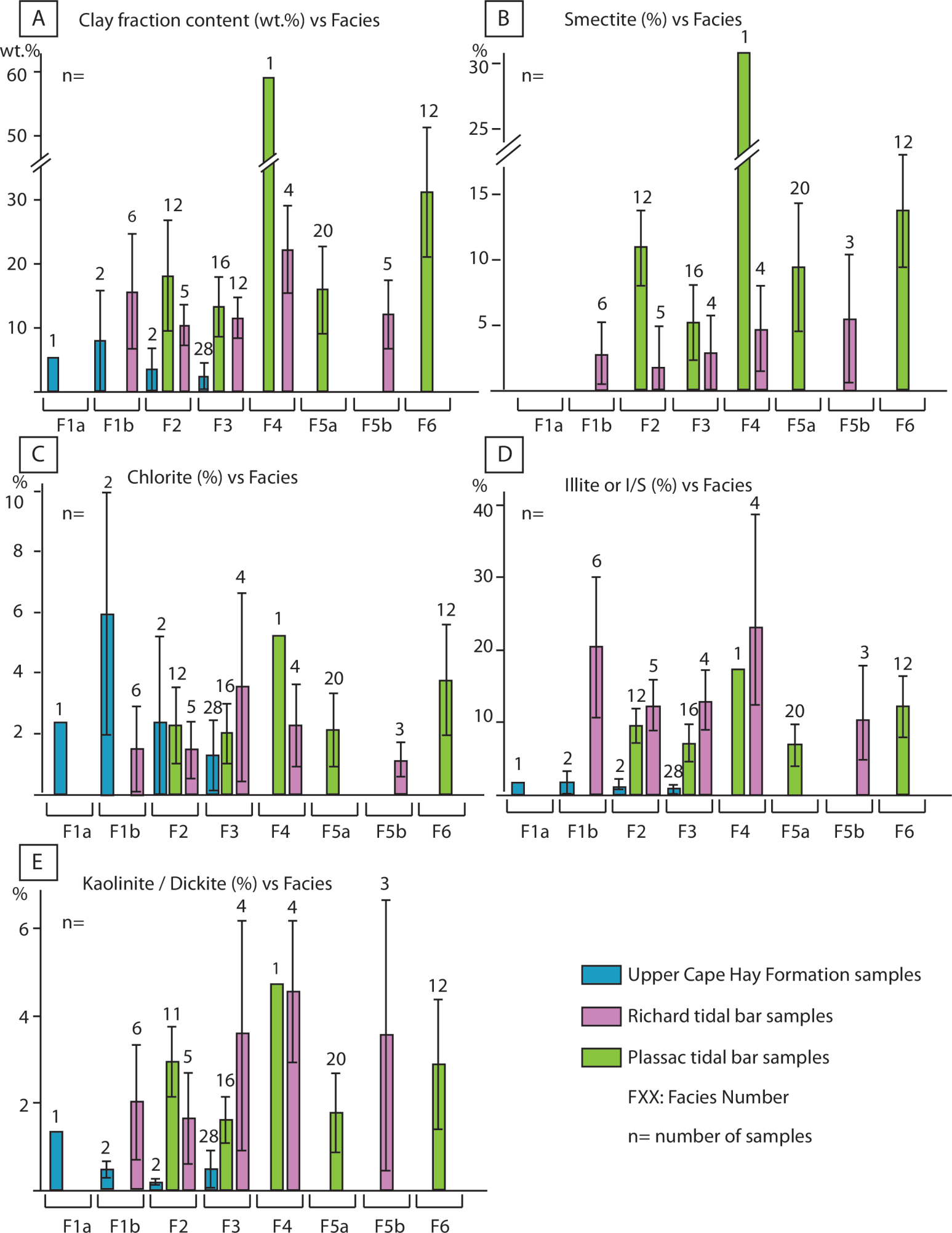
A
Clay fraction content (wt.%) vs Facies
wt.%
n=
B
Smectite (%) vs Facies
%
n=
C
Chlorite (%) vs Facies
%
n=
D
Illite or I/S (%) vs Facies
%
n=
E
Kaolinite / Dickite (%) vs Facies
%
n=
F1a
F1b
F2
F3
F4
F5a
F5b
F6
Upper Cape Hay Formation samples
Richard tidal bar samples
Plassac tidal bar samples
FXX: Facies Number
n= number of samples

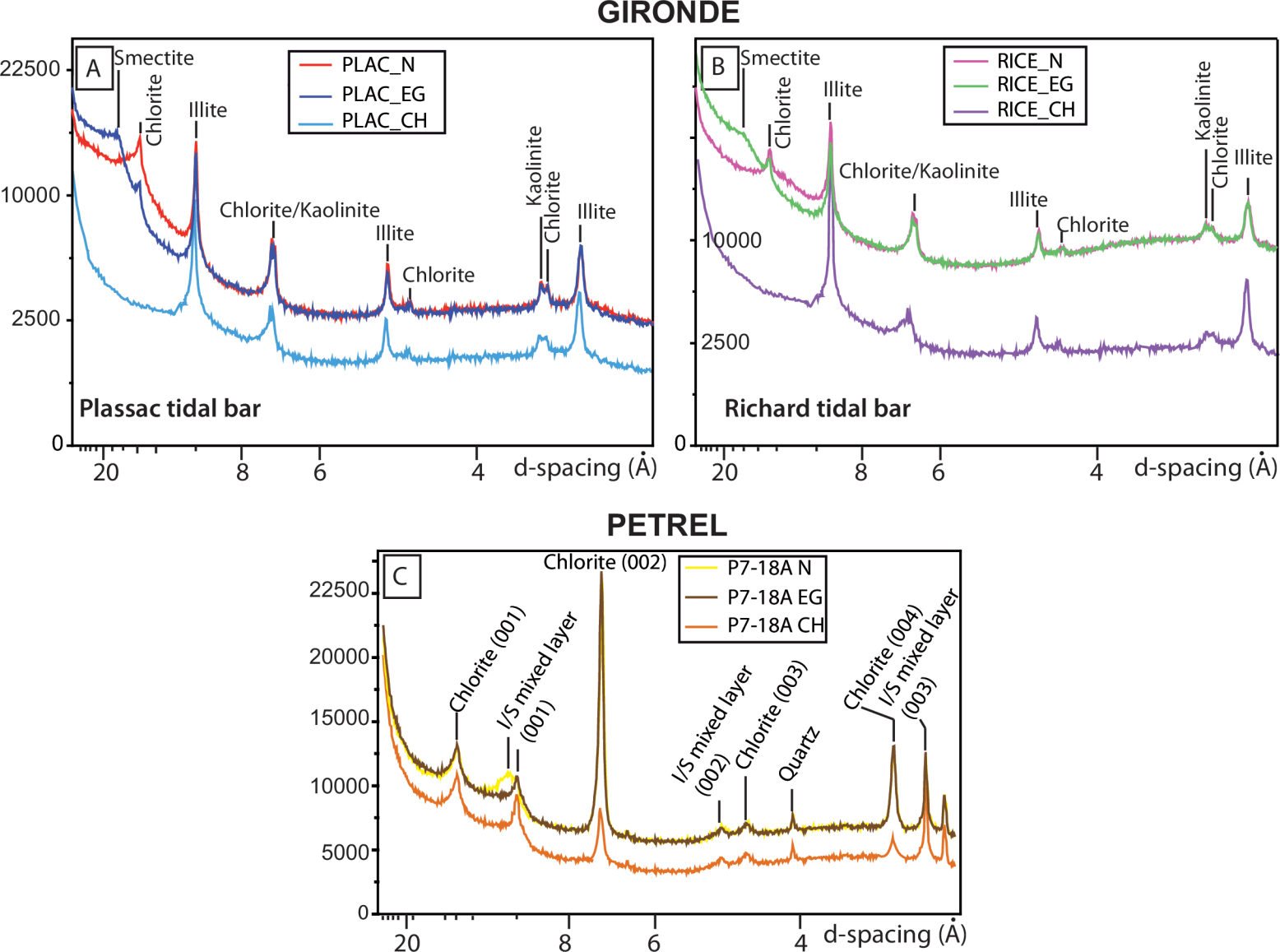
GIRONDE
A
Smectite
Chlorite
Illite
PLAC_N
PLAC_EG
PLAC_CH
Chlorite/Kaolinite
Illite
Chlorite
Kaolinite
Chlorite
Illite
22500
10000
2500
0
Plassac tidal bar
20
8
6
4
d-spacing (Å)
B
Smectite
Chlorite
Illite
RICE_N
RICE_EG
RICE_CH
Chlorite/Kaolinite
Illite
Chlorite
Kaolinite
Chlorite
Illite
10000
2500
0
Richard tidal bar
20
8
6
4
d-spacing (Å)
PETREL
C
Chlorite (002)
P7-18A N
P7-18A EG
P7-18A CH
Chlorite (001)
I/S mixed layer (001)
I/S mixed layer (002)
Chlorite (003)
Quartz
Chlorite (004)
I/S mixed layer (003)
22500
20000
15000
10000
5000
0
20
8
6
4
d-spacing (Å)

GIRONDE = MODERN SANDSTONE

PETREL = BURIED SANDSTONE

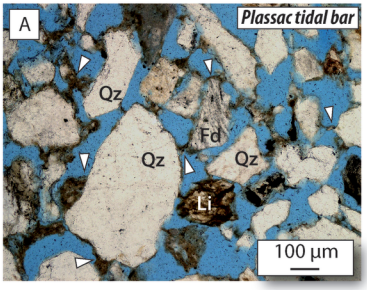

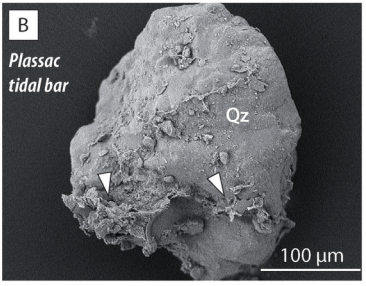

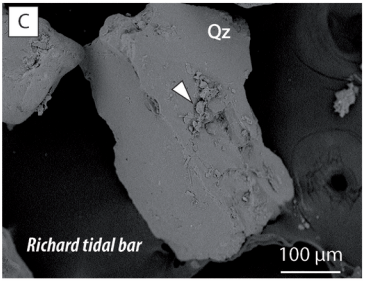

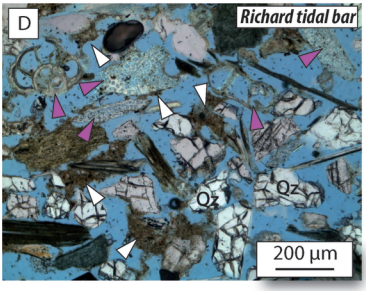

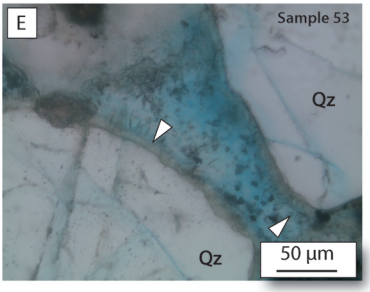

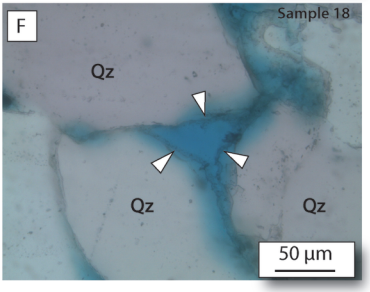

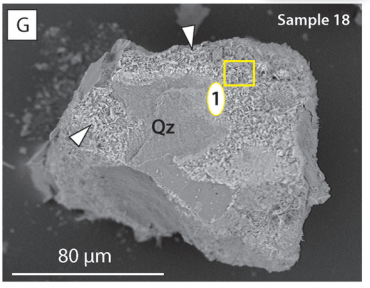

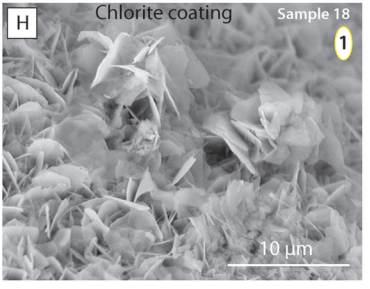

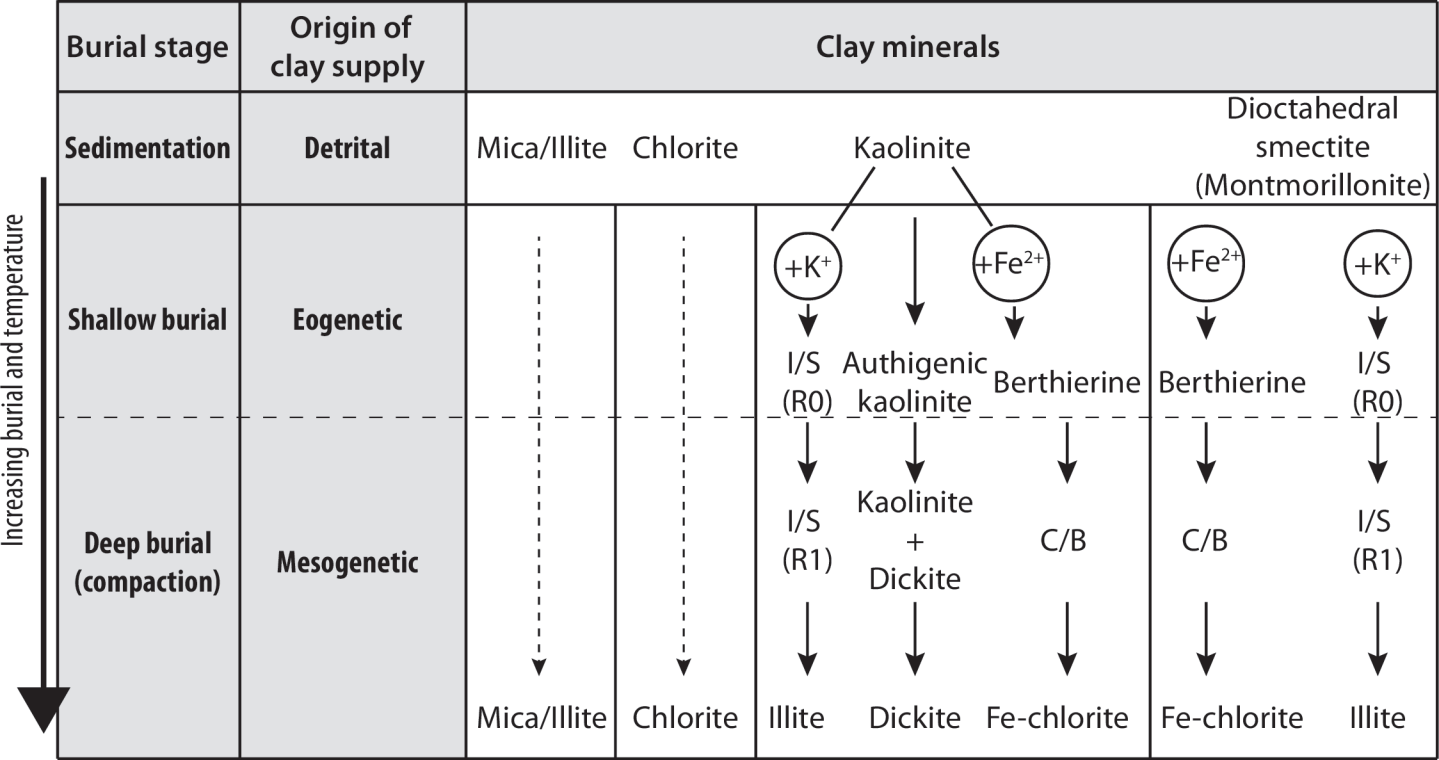
Burial stage
Origin of clay supply
Clay minerals
Sedimentation
Detrital
Mica/Illite
Chlorite
Kaolinite
Dioctahedral smectite (Montmorillonite)
Shallow burial
Eogenetic
+K+
+Fe2+
+Fe2+
+K+
I/S (R0)
Authigenic kaolinite
Berthierine
Berthierine
I/S (R0)
Deep burial (compaction)
Mesogenetic
I/S (R1)
Kaolinite + Dickite
C/B
C/B
I/S (R1)
Mica/Illite
Chlorite
Illite
Dickite
Fe-chlorite
Fe-chlorite
Illite
Increasing burial and temperature

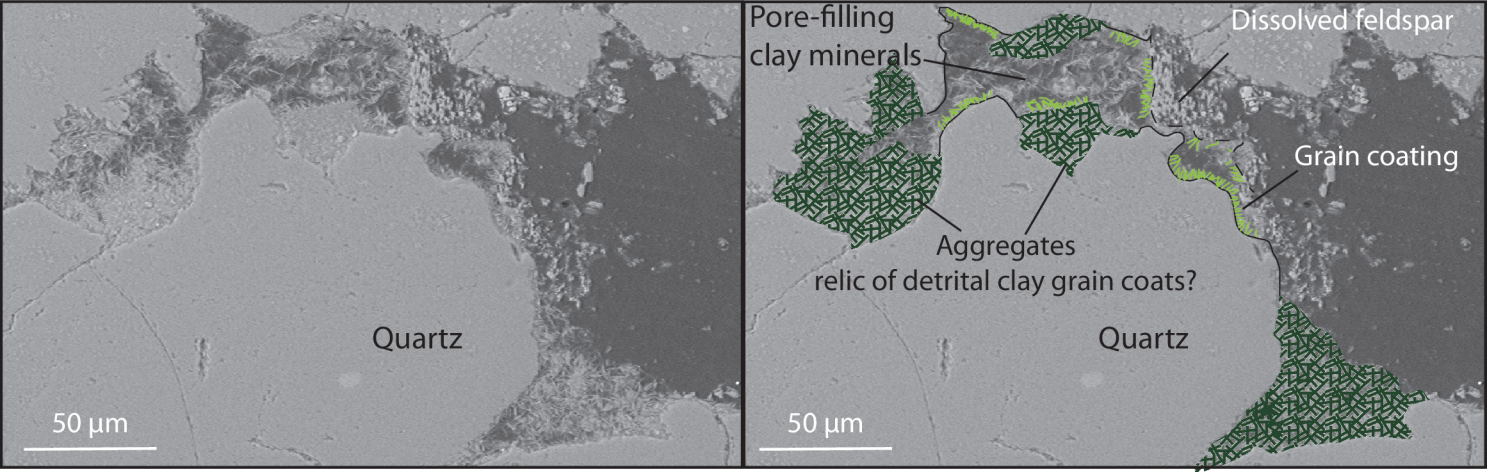
Quartz
50 µm
Pore-filling
clay minerals
Dissolved feldspar
Grain coating
Aggregates
relic of detrital clay grain coats?
Quartz
50 µm

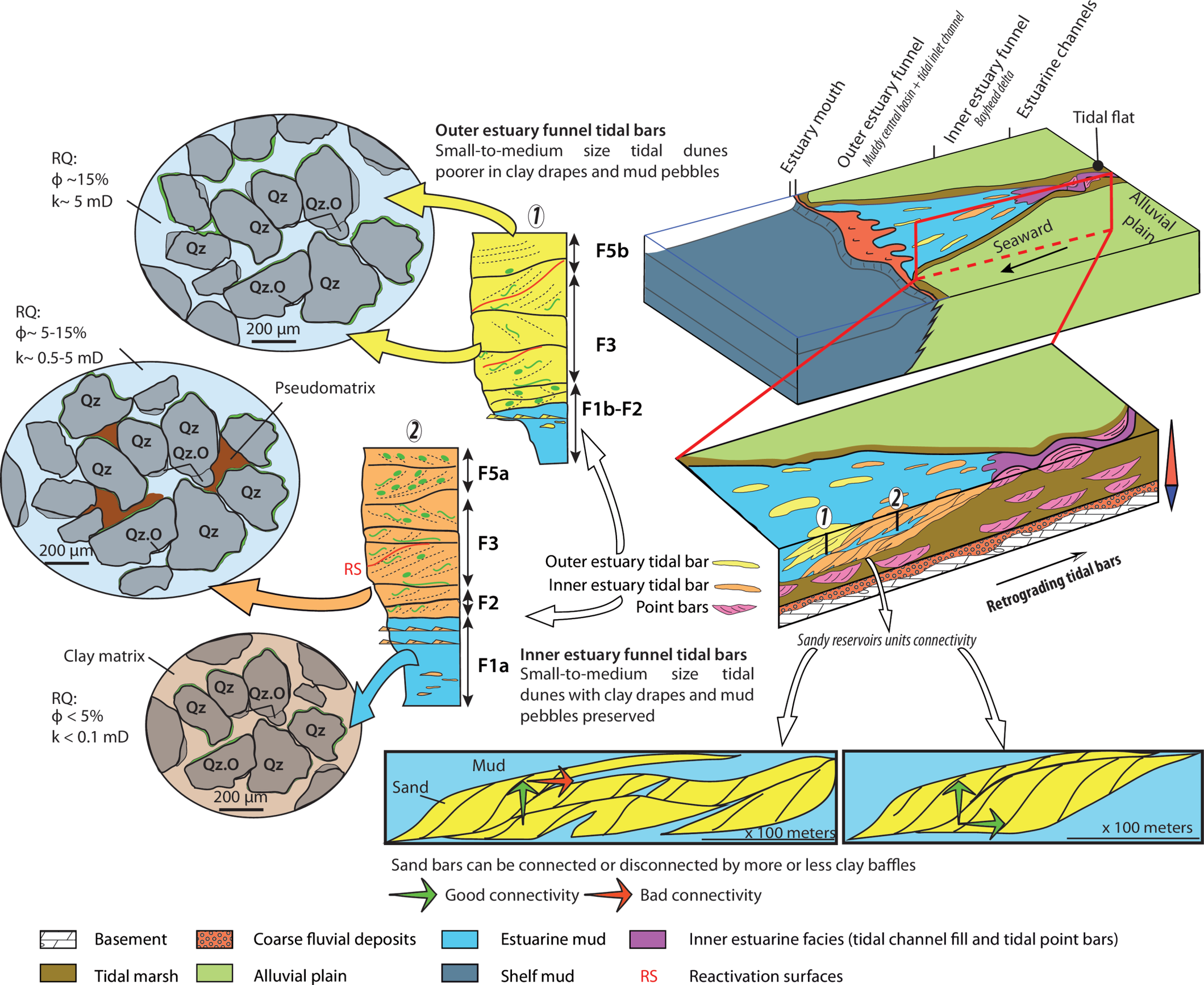
Estuary mouth
Outer estuary funnel
Muddy central basin + tidal inlet channel
Inner estuary funnel
Bayhead delta
Estuarine channels
Tidal flat
Alluvial plain
Seaward
Retrograding tidal bars
Sandy reservoirs units connectivity
Outer estuary funnel tidal bars
Small-to-medium size tidal dunes poorer in clay drapes and mud pebbles
RQ:
ϕ ~15%
k~ 5 mD
Qz
Qz.O
200 µm
RQ:
ϕ~ 5-15%
k~ 0.5-5 mD
Pseudomatrix
RQ:
ϕ < 5%
k < 0.1 mD
Clay matrix
F5b
F3
F1b-F2
F5a
F2
F1a
RS
Outer estuary tidal bar
Inner estuary tidal bar
Point bars
Inner estuary funnel tidal bars
Small-to-medium size tidal dunes with clay drapes and mud pebbles preserved
Mud
Sand
x 100 meters
Sand bars can be connected or disconnected by more or less clay baffles
Good connectivity
Bad connectivity
Basement
Coarse fluvial deposits
Estuarine mud
Inner estuarine facies (tidal channel fill and tidal point bars)
Tidal marsh
Alluvial plain
Shelf mud
RS
Reactivation surfaces

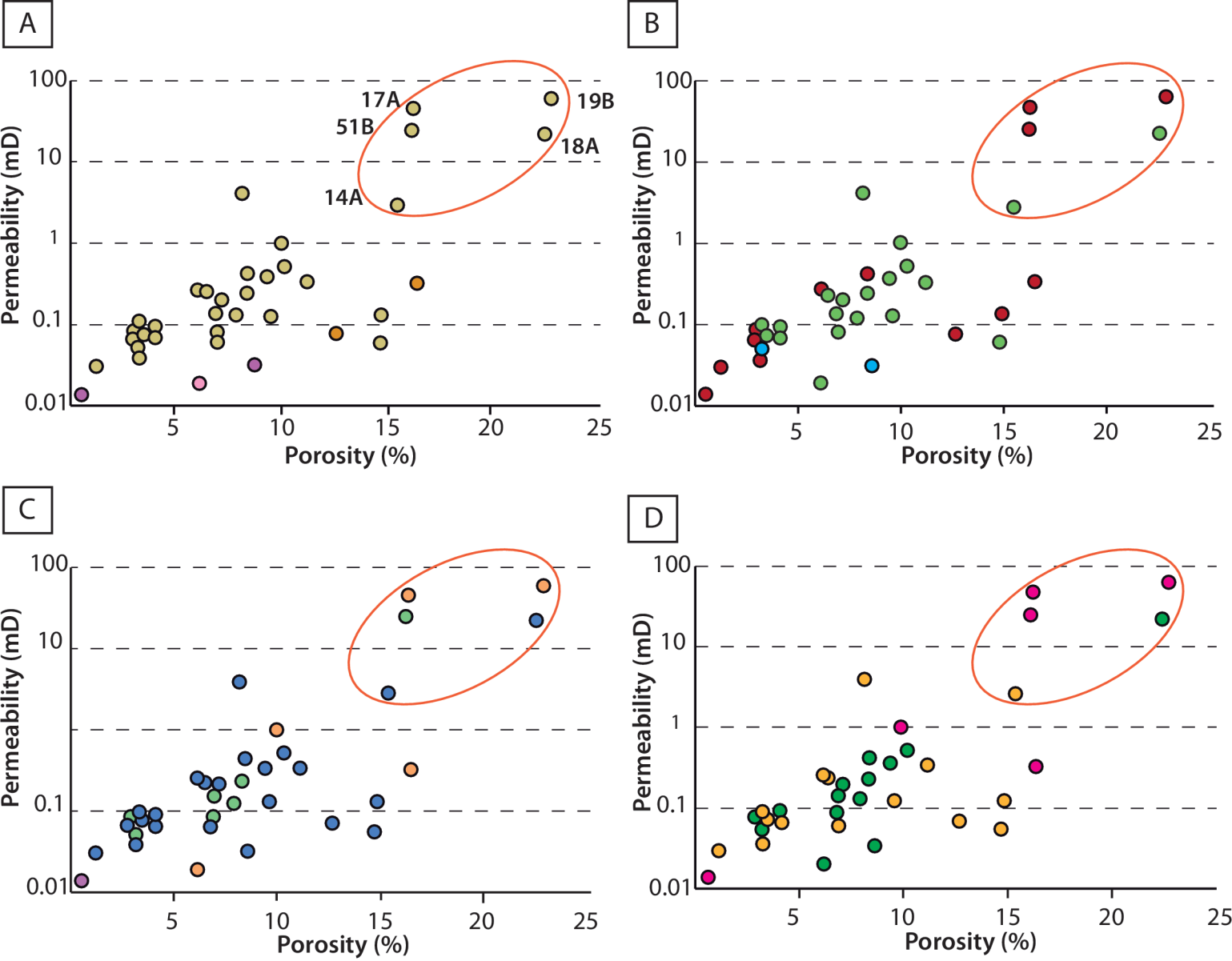

Legend A:

F1a F1b F2 F3 XX A-B: sample number (cf synthetic log)

Legend B:

Coated grain content: Lower than 60% Between 60% and 70% Higher than 70%

Legend C:

Clay fraction content: Between 0 and 3 wt% Between 3 and 5 wt% Between 5 and 10 wt% Higher than 10 wt%

Legend D:

Chlorite content: Lower than 1% Between 1% and 2% Higher than 2%

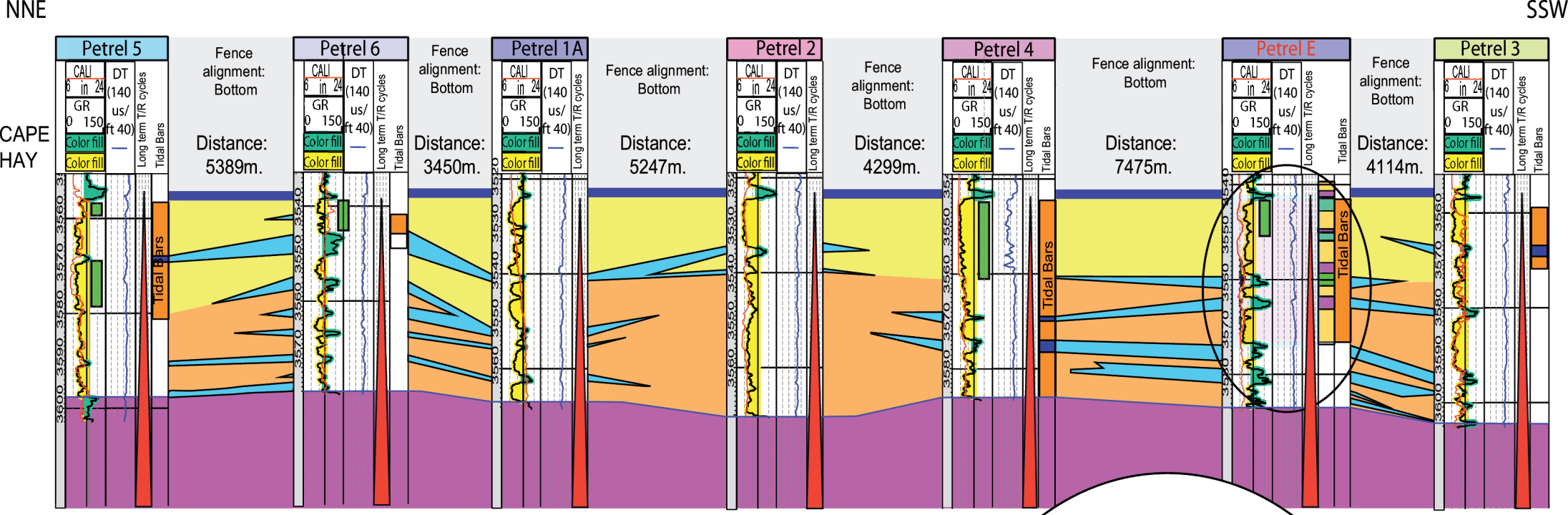

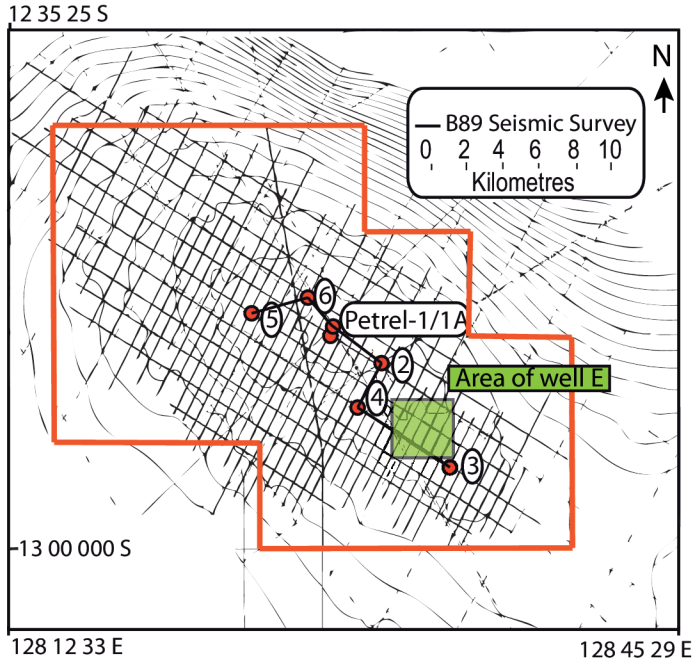

Correlation transect and well locations within the Petrel sub-basin (from Kloss et al., 2004)

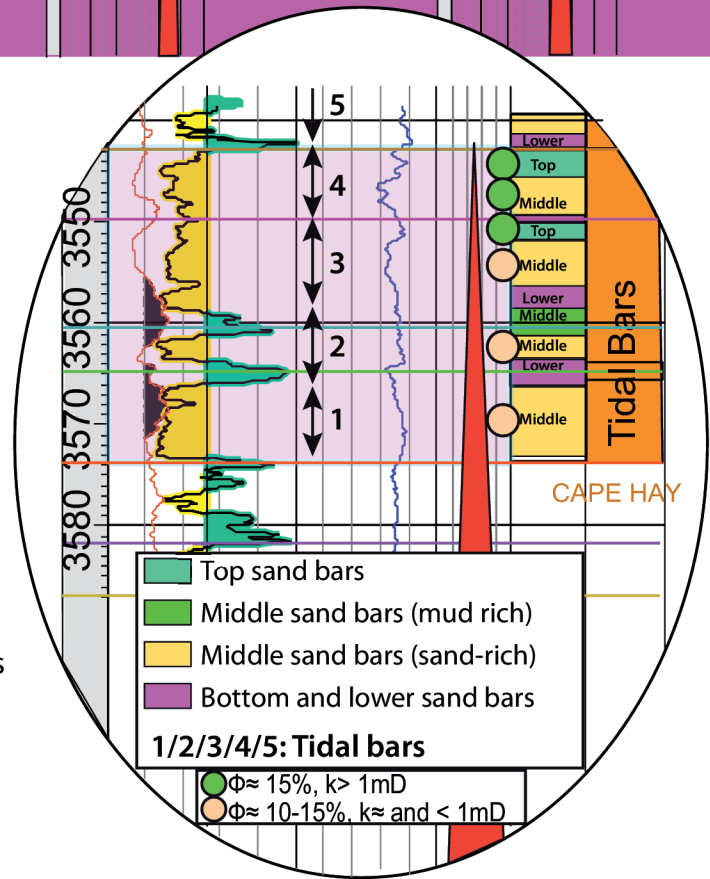

Facies number	Facies name	Location area	Facies description	Texture	Thickness	Set thickness	Location in the bar
F1	Fluid mud facies	Plassac tidal bar and Petrel deposits	F1a: Mud matrix with rhythmic layering where groups of sandy ripples alternate with groups of linsens in a cyclic pattern, suggesting a neap-spring cycle layering	Petrel: mean grain size of 116 µm	Decimeter to meter thick	/	Bottom of the tidal bars
		Richard tidal bar and Petrel deposits	F1b: Homogeneous fluid mud layers, sometime associated with very thin layers of fine-grained linsens and sandy ripples	Fluid mud Richard: mean grain size of ripples of 183 µm Petrel: mean grain size of 151 µm	Centimeter to decimeter thick	/	
F2	Lower sand bar facies	Richard, Plassac tidal bars and Petrel deposits	Medium-to-fine grained small size dunes with more or less abundant and thick mud pebbles or clay drapes on foresets and bottomsets Sometimes, an alternation of centimeter thick beds of fine-grained ripples and millieter-to centimeter-thick clay drapes is observed Organic matter rich layers are observed in Richard tidal bar (leaves, wood) Bi-directionnality badly expressed Counter currents reactivation surfaces and clay drapes couplets	Richard: mean grain size of 185 µm Plassac: mean grain size of 231 µm Petrel: mean grain size of 176 µm	Decimeter to meter thick	Richard: mean thickness of 12 cm Plassac: mean thickness of 10 cm Petrel: mean thickness of 8.5 cm	Lower sand bar
F3	Middle sand bar facies	Richard, Plassac tidal bars and Petrel deposits	Medium-to-fine grained small-to-medium size dunes with thin clay drapes or mud pebbles on foresets Sometimes, foresets display low-angular to sub-planar cross-stratification Thin bottomsets composed by horizontal clay drapes Some counter current reactivation surfaces and clay drape couplets Bi-directionality badly expressed Possible bioturbation in bottomsets	Richard: mean grain size of 198 µm Plassac: mean grain size of 220 µm Petrel: mean grain size of 156 µm	Decimeter to meter thick	Richard: mean thickness of 10 cm Plassac: mean thickness of 23 cm Petrel: mean thickness of 10 cm	Middle sand bar
F4	Middle bar muddy facies	Richard, Plassac tidal bars and Petrel deposits	Millimetric alternations of thinly-bedded fine grained silty linsens to centimeter-thick ripples with amalgamated clay drapes or muddy layers Millimetric to centimetric clay drapes	Richard: mean grain size of 132 µm	Decimeter to meter thick	/	
F5	Upper sand bar facies	Plassac tidal bar and Petrel deposits	F5a: Medium-to-fine grained, small-to-medium size dunes with abundant mud pebbles on foresets Thin bottomsets with horizontal clay drapes and mud pebbles Bi-directionnality badly expressed Counter currents reactivation surfaces and clay drapes couplets	Mean grain size on Plassac: 252 µm	Decimeter to meter thick	Plassac: mean thickness of 10 cm Petrel:mean thickness of 7 cm	Upper sand bar
		Richard tidal bar	F5b: Fine grained small-size dunes with rare clay drapes or mud pebbles on foresets and bottomsets	Mean grain size of 213 µm	Decimeter to meter thick	/	
F8	Tidal flat facies	Plassac tidal bar	Three types of beddings are vertically stacked: Lenticular bedding, Wavy bedding, Flaser bedding Rare small size tidal dunes with thick mud pebbles or clay drapes on foresets and bottomsets Possible bioturbation	Mean grain size: 208 µm	Meter thick	/	Tidal flat

Table 1

Facies		Tidal bars	Petrographic Samples	Mineralogical samples	Grains (%)							Coat coverage (%)	Cement (%)	Porosity (%)	Mean grain size (μm)	Clay fraction (wt%)	Clay minerals content (%)			
					Total quartz	Total feldspar	Total lithics	Pyrite	Various	Total	Total coated [illegible]						Smectite	Chlorite	Illite I/S	Kaolinite/ Dickite
F1	F1a	Petrel	1	1	63	7	3	0	0	73	60	48	26	6	116	5	0.0	2.4	1.6	1.3
		Plassac	/	/	/	/	/	/	/	/	/	/	/	/	/	/	/	/	/	/
		Richard	/	/	/	/	/	/	/	/	/	/	/	/	/	/	/	/	/	/
	F1b	Petrel	2	2	66	9	1	1	0	76	64	61	19	5	151	8	0.0	6.0	1.6	0.5
		Plassac	/	/	/	/	/	/	/	/	/	/	/	/	/	/	/	/	/	/
		Richard	3	6	36	7	12	1	10	66	19	15	/	16	183	29	4	2	14	2
F2	F2	Petrel	1	2	70	7	0	1	0	78	73	71	4	14	176	4	0.0	2.4	1.0	0.2
		Plassac	8	12	33	6	18	0	8	66	24	25	/	15	231	25	11.0	2.0	9.0	3.0
		Richard	8	10	39	7	18	1	12	76	18	5	/	14	185	21	2.0	2.0	20.0	2.0
F3	F3	Petrel	23	28	65	7	2	1	0	76	68	64	10	12	156	3	0.0	1.1	0.6	0.4
		Plassac	16	20	40	9	15	0	8	72	26	20	/	14	220	15	5	2	7	2
		Richard	12	12	37	6	17	0	17	78	17	5	/	13	198	14	3	4	13	4
F4	F4	Petrel	0	0	/	/	/	/	/	/	/	/	/	/	/	/	/	/	/	/
		Plassac	/	1	/	/	/	/	/	/	/	/	/	/	/	58	31	5	17	5
		Richard	4	4	28	5	18	1	16	67	18	15	/	13	132	37	5	2	23	5
F5	F5a	Petrel	0	0	/	/	/	/	/	/	/	/	/	/	/	/	/	/	/	/
		Plassac	20	22	35	8	19	0	8	71	29	15	/	15	252	20	9	2	7	2
		Richard	/	/	/	/	/	/	/	/	/	/	/	/	/	/	/	/	/	/
	F5b	Petrel	/	/	/	/	/	/	/	/	/	/	/	/	/	/	/	/	/	/
		Plassac	/	/	/	/	/	/	/	/	/	/	/	/	/	/	/	/	/	/
		Richard	5	9	39	6	13	0	17	75	14	15	/	15	213	17	3	1	10	1
F6	F6	Petrel	/	/	/	/	/	/	/	/	/	/	/	/	/	/	/	/	/	/
		Plassac	8	12	30	7	12	0	8	58	22	15	/	13	208	34	15	4	12	3
		Richard	/	/	/	/	/	/	/	/	/	/	/	/	/	/	/	/	/	/
Average		Petrel	/	/	66	7	2	1	0	76	66	61	15	9	150	5	0	4	1	1
		Plassac	/	/	34	8	16	0	8	67	25	19	/	14	228	30	14	3	10	3
		Richard	/	/	36	6	15	1	14	73	17	11	/	14	182	24	3	2	16	3

Table 2